Multimodal profiling of human sensory neurons links electrical properties to transcriptional identity

Short title: Multimodal profiling of human DRG using Patch-seq

Authors

Jiwon Yi[1, 2], Lite Yang[1,2], Allie J. Widman[1], Alexa Toliver[1], Zachariah Bertels[1†], John Smith Del Rosario[1†], Adam J. Dourson[1†], Prashant Gupta[1†], Rakesh Kumar[1†], Jun-Nan Li[1†], Maria Payne[1†], Richard A. Slivicki[1†], Juliet M. Mwirigi[1], Alexander Chamessian[1], Kesav Kothapalli[1], Grace Moore[1], John Lemen[3], Bryan A. Copits[1*], Robert W. Gereau IV[1,4*], PRECISION Human Pain Network

Affiliations

[1] Department of Anesthesiology, Washington University Pain Center, Washington University School of Medicine, St. Louis, MO, United States

[2] Neuroscience Graduate Program, Division of Biology & Biomedical Sciences, Washington University School of Medicine, St. Louis, MO, United States

[3] Mid-America Transplant, St. Louis, MO, United States

[4] Department of Neuroscience, Washington University in St. Louis, St. Louis, MO, United States

[†]These authors contributed equally to this work.

*Corresponding authors. Address: Department of Anesthesiology, Washington University Pain Center, Washington University School of Medicine, 660 South Euclid Avenue Campus Box 8054, St. Louis, 63110, MO, United States. E-mail: bcopits@wustl.edu (B.A. Copits) and gereaur@wustl.edu (R.W. Gereau). Phone: (314) 362-8312. URL: pain.wustl.edu

Abstract

Despite major advances in pain science, the approval of novel therapeutics has been slow. A major cause for the lack of new analgesics may be fundamental biological differences between humans and model organisms used in preclinical research. Large-scale transcriptional profiling efforts on human dorsal root ganglia (hDRG) have now identified at least 22 distinct neuronal subtypes; however, a significant knowledge gap exists in ascribing functional phenotypes to these diverse neuronal populations. In this study, we use Patch-seq recordings in hDRG to link electrical properties to transcriptionally defined cell types. First, through unbiased clustering of electrophysiological properties from 228 hDRG neurons, we identify three electrophysiological subtypes (E-types). Next, we show that E-types can be mapped onto specific transcriptional classes (T-types) of hDRG neurons. We find that donor's pain history is associated with E-type-specific differences in electrical properties, some of which may be associated with higher expression of voltage-gated sodium channels, NaV1.7 and NaV1.8. These results highlight the importance of using multimodal profiling to better understand human sensory neuron biology and may help reveal novel therapeutic targets driving chronic pain.

Teaser

Mapping electrical properties to transcriptional profiles of human sensory neurons offers new insights into pain neurobiology

Introduction

Chronic pain affects an estimated 20% of people worldwide, resulting in disability, reduced quality of life, and the dearth of treatment options is a major driver of the current opioid epidemic in the U.S.(*1–4*). While a multitude of potential new analgesic targets have been identified in preclinical studies in animal models, the vast majority of efforts to translate these findings into new treatments have failed in clinical trials. As such, available options for non-opioid pharmacotherapy in patients are still limited(*5*). While there are many possible reasons that translational efforts in pain fail so frequently, it is becoming increasingly apparent that a poor understanding of the relationship between human physiology and that of animals used in preclinical studies is a major contributor. Understanding the cellular identity and physiology of human sensory neurons and how these differ in the context of painful conditions is therefore critical to better translate preclinical findings from rodents to humans and to identify unique properties of human sensory neurons that can be targeted for therapeutic development. Collecting this type of information is the current goal of the NIH HEAL Initiative's PRECISION human pain network (*6*). Here, we describe progress on one PRECISION network study where we seek to identify diverse electrophysiological phenotypes of human sensory neurons from the dorsal root ganglion (DRG), map these properties onto genetically identified cell types and understand differences in physiology and gene expression seen in the context of chronic pain.

Nociceptor hyperactivity following injury or inflammation is a critical driver in the development and/or maintenance of pain (*7*, *8*), and both C-fiber and A-fiber nociceptors display ectopic spontaneous activity and hyperexcitability in animal models of neuropathic, inflammatory, and chemotherapy-induced pain. The relevance of these findings is further bolstered by the observation that human dorsal root ganglia (hDRG) neurons from patients with neuropathic pain are much more likely to have spontaneous activity (*9–11*). Whether similar pain-associated hyperexcitability of hDRG neurons is seen in other pain conditions, such as musculoskeletal pain, is yet unknown. Interestingly, in a rat model of neuropathic pain, nociceptor sensitization is only seen in neurons that have non-accommodating (repetitively firing) spike patterns, but not in rapidly accommodating (single spiking) nociceptors (*12*). Similarly, bradykinin-induced hyperexcitability of hDRG neurons varies between repetitively firing and single spiking neurons (*13*). These findings suggest that certain electrophysiological features are associated with cell types that are sensitized in the context of pain-inducing injury or inflammation.

A wealth of studies in rodent DRG has revealed that nociceptors themselves are a heterogenous population that consist of multiple specialized sub-populations defined by distinct chemo- and mechano-sensitivities, transcriptional profiles, developmental regulation, and projection patterns (*14*–*25*). Molecularly defined subpopulations of mouse nociceptors display distinct intrinsic membrane properties, suggesting that transcriptional profiles and physiological properties are linked (*25*, *26*). While single-cell transcriptomics studies using hDRG show that core functional groups of sensory neurons appear conserved from rodents to humans, the relative proportion of different functional populations differ across species (*27*–*30*). Compared to rodent, hDRG neurons also more broadly express nociceptive receptors, ion channels, and neuropeptides (*31*–*37*), contain a higher proportion of chemosensitive neurons, and have different intrinsic membrane properties and spike kinetics (*38*). However, a multimodal characterization linking the transcriptional and physiological characteristics of human sensory neurons is currently lacking.

In this study, we address this gap by combining patch-clamp electrophysiology paired with single-cell RNA sequencing (Patch-seq (*39*)) in hDRG neurons obtained from postmortem organ donors. By profiling the excitability of over 200 hDRG neurons obtained from 56 donors, we identify three electrophysiological subtypes (E-types) of hDRG neurons that show distinct membrane properties and spike kinetics. We identify four transcriptional hDRG neuronal classes (T-types), which E-types can be broadly mapped onto. Next, we utilize sub-group analysis to show that hDRG neurons from donors with pain history demonstrate E-type dependent differences in spike kinetic properties and differential expression of ion channels. Together, these findings suggest that hDRG neurons show physiological specialization which may be associated with functional diversity and illustrate ways in which the large-scale collection of these types of multimodal data can generate insights into potential underlying causes of chronic pain to spur new therapeutic development.

Results

Unbiased clustering of small- to medium-size human somatosensory neurons based on physiological characteristics

Rodent sensory neurons can be organized into clusters that share similar physiological characteristics, and these clusters are associated with distinct transcriptional profiles and molecularly defined subpopulations of sensory neurons (*12*, *25*, *26*, *40*). Here, we tested whether such physiological heterogeneity also exists in hDRG neurons *in vitro*. Using primary culture of hDRG obtained from postmortem organ donors (**Table 1, Table S1**), we performed patch-clamp experiments to assess the membrane excitability of hDRG neurons. As prior work has demonstrated enrichment of human nociceptor populations among smaller diameter sensory neurons, whereas non-nociceptive subtypes like proprioceptors and low threshold mechanoreceptors are found in hDRG neurons with larger soma size (*33*, *34*) we focused our investigation on small- to medium-sized hDRG neurons (mean cell diameter ± SD: 40.65 ± 11.23μm). A small percentage of patch-clamp recordings (4.8%) were performed on larger hDRG neurons with diameter >60μm (**Fig. 1A**). To determine if different hDRG cell types exhibit distinct electrical properties, we extracted 10 electrophysiological features from 228 hDRG recordings (**Fig. 1B-D)**.

To classify the electrophysiological phenotypes (E-types) of hDRG neurons in an unbiased manner, we used principal component analysis (PCA) to cluster hDRG neurons based on their electrical properties (n=228; **Fig. 1E, F**). Features related to action potential (AP) kinetics, such as peak, decay time, and half-width, and features associated with intrinsic excitability, such as rheobase (the minimum current threshold required to fire an action potential), were found to have the largest contributions to the principal components (**Fig. 1E**). Using K-means neighbor clustering (**Fig. S1**), hDRG neurons were separated into three clusters: E-type 1, 2, and 3 (**Fig. 1F**). E-type 3 represented the largest cluster, made up of over half (121/228, or 53.07%) of the hDRG neurons patched. Approximately one-third (74/228, or 32.46%) of hDRG neurons were assigned to E-type 2, whereas E-type 1 consisted of a minority of hDRG neurons (33/228, or 14.47%; **Fig. 1G**). There were no significant associations between number of days in culture and the relative proportion of each E-type (**Fig. S2**). The membrane properties and action potential kinetics of the three E-types are summarized in **Table 2**.

Our PCA highlighted features associated with spike waveform and kinetics that contributed to clustering into three E-types (**Fig. 1E**). Analysis of the AP waveform kinetics (**Fig. 1C, H-N**)

133 revealed that E-type 2 exhibits action potentials with significantly wider half-widths and a slower
134 decay phase than both E-types 1 and 3 (**Fig. 1J, L**). While both E-types 1 and 3 were
135 characterized by narrow action potential spikes with a fast decay phase (**Fig. 1H-J, K**), E-type 1
136 could be distinguished from E-type 3 based on its low peak and amplitude (**Fig. 1H, M, N**), as well
137 as the slowest rise time of the three E-types (**Fig. 1I, K**). Together, these results suggest that
138 hDRG neurons can be functionally clustered based on their membrane properties and spike
139 kinetics.

140 ## Human somatosensory neurons exhibit distinct high- and low-excitability E-types

141 Studies in both mouse and rat have reported at least 2-3 different firing subtypes within
142 the small-diameter nociceptor population: one cluster that shows a non-repetitive, single-firing
143 phenotype, and another that displays a repetitive firing pattern (*12*, *25*). These clusters may
144 represent unique transcriptionally defined and functionally distinct subpopulations of
145 somatosensory neurons (*25*). Additionally, these clusters have been hypothesized to represent
146 different functional states of nociceptors, as the relative proportion of these clusters can change
147 in response to nerve injury (*12*) or inflammatory mediators (*13*). Therefore, we analyzed if each
148 hDRG E-type was associated with a distinct action potential firing pattern and excitability
149 phenotype.

150 First, E-type 2 hDRG neurons fired action potentials in response to significantly lower
151 current injections (**Fig. 2A-D**) and exhibited a significantly higher input resistance compared to E-
152 types 1 and 3 (**Fig. S3A, B**), consistent with higher excitability. In contrast, hDRG neurons with
153 E-type 3 had significantly higher rheobase than E-type 2 and exhibited the lowest input resistance,
154 largest voltage sag, and the most hyperpolarized resting membrane potential out of the three (**Fig.**
155 **S3B-D**), suggestive of low membrane excitability. Additionally, hDRG neurons with E-type 3 had
156 a significantly larger cell diameter than neurons with E-type 2 (E-type 3 vs. E-type 2, 43.07μm ±
157 1.055 vs. 36.85 μm ± 0.97; **Fig. S4**).

158 Next, to determine each spike firing pattern, we analyzed the AP spike output to
159 suprathreshold current injections (**Fig. 2E, F**). To determine the spike firing phenotypes across
160 these three E-types, we classified neurons as multi-spiking (>1 action potential fired at up to 3x
161 rheobase) or single-spiking (no more than 1 action potential fired at up to 3x rheobase). We
162 observed that a subset of hDRG neurons had a significantly higher rheobase (1707 ± 90.9pA, **Fig.**
163 **2D, Table S2**) which limited us from testing their spike output at 3x rheobase; these neurons were
164 classified as "high rheobase." The relative proportions of multi-spiking, single-spiking, and high

165 rheobase neurons were significantly different across the three E-types (**Fig. 2G**).

166 Analysis of spiking patterns revealed that E-type 2 fire a significantly higher number of
167 action potentials at suprathreshold currents compared to E-types 1 and 3 (**Fig. 2A-C, E, F**), and
168 E-type 2 neurons were predominantly composed of multi-spiking neurons (65/74, or 87.84%; **Fig.**
169 **2G**). In contrast, less than 25% of hDRG neurons with either E-type 1 (21.21%, or 7/33 neurons)
170 or E-type 3 (23.97%, or 29/121 neurons) exhibited a multi-spiking pattern (**Fig. 2G**). E-type 3
171 neurons were most likely to be single-spikers (74/121, or 61.16%, **Fig. 2E-G**), whereas E-type 1
172 neurons were composed of both single-spiking (15/33 neurons, or 45.45%; **Fig. 2E-G**) and high
173 rheobase neurons (11/33 neurons, or 33.33%; **Fig. 2G**). Together, these results suggest that E-
174 type 2 represents a high-excitability, low-threshold, multi-spiking phenotype of human
175 somatosensory neurons, whereas E-type 1 and 3 may represent populations of human sensory
176 neurons with high activation thresholds.

177 Patch-seq identifies four T-types of human DRG neurons

178 Recent scRNA-seq studies have revealed up to 22 transcriptionally distinct hDRG sensory
179 neuronal subtypes, which can be broadly grouped into several major classes: A-fiber low
180 threshold mechanoreceptors (A-LTMR), proprioceptors, A-fiber peptidergic neurons (A-PEP), C-
181 fiber non-canonical peptidergic neurons (C-NP), and C-fiber peptidergic neurons (C-PEP) (*37*).
182 However, it remains unknown whether distinct firing patterns are linked to specific transcriptionally
183 defined populations (*1–4*). We thus performed Patch-seq recordings that allowed us to examine
184 the relationship between E-types and transcriptional types or T-types from the same cultured
185 hDRG cells (*39*). After patch-clamp recording, we performed RNA-seq on the cytosolic contents
186 extracted from individually recorded cells (**Fig. 3A, Fig. S5A**). We established cDNA quality
187 control (QC) metrics to identify high quality samples (**Methods, Fig. S5B**). Samples that passed
188 the cDNA QC showed significantly more reads mapped to human genome and transcripts
189 detected compared to those that failed QC (**Fig. S5C**). In total, we collected and processed 310
190 Patch-seq samples, and 139 passed QC metrics and thus were included in the transcriptional
191 analysis.

192 Despite recent efforts to elucidate the transcriptional profiles of diverse hDRG neuronal
193 types, the evidence to provide the ground truth about their cytosolic RNA diversity is lacking as
194 the majority of studies have focused on nuclear transcripts. We compared the average expression
195 of all detected genes across Patch-seq samples to the average expression of those genes across
196 neurons and non-neuronal cells from several hDRG single cell atlases previously reported,

197 generated using varying input (e.g. single-nucleus, single-cell, and single-soma; **Fig. S5D**)(*28*, *32*,
198 *34*, *36*, *41*). Consistent with their similarity in RNA origin, the transcriptional profile of the hDRG
199 Patch-seq data best correlated to that of the hDRG single-soma RNA-seq data (*41*). Therefore,
200 we used the cell type annotation and the marker genes identified from the single-soma RNA-seq
201 data (*41*) to guide our transcriptional analysis.

202 To study the transcriptional identity of hDRG Patch-seq samples, we first performed
203 clustering analysis that revealed four transcriptionally distinct clusters (**Fig. S6A**). Using the
204 marker genes previously reported (*42*, *47*), we mapped each cluster to major human DRG cell
205 classes (*36*, *42*). Cluster 1 to 3 express neuronal marker genes, such as *SNAP25* and *RBFOX3*,
206 and are transcriptionally similar to hDRG neuronal cells, whereas cluster 4 expresses non-
207 neuronal marker gene *APOE* and is transcriptionally more similar to non-neuronal cells previously
208 described (**Fig. S6B, C**). Based on the expression of cell-type-specific DRG transcription factors
209 and other canonical marker genes, clusters 2 and 3 likely correspond to A-PEP and C-PEP
210 neurons, respectively, and cluster 1 appears to consist of transcriptionally distinct populations that
211 match with *NTRK3*-expressing A-LTMR and *PRDM12*-expressing C-NP neurons (**Fig. S6D**).
212 Notably, neuronal clusters also express injury-associated genes, such as *ATF3* and *SOX11*, which
213 are likely induced by the cell dissociation and culture process (*43*). To better separate
214 transcriptionally distinct hDRG neuronal classes, we next integrated the 126 Patch-seq samples
215 from the neuronal clusters (clusters 1-3) to hDRG single-soma RNA-seq data and annotated their
216 T-types by label transfer (**Fig. 3B**). T-type annotation largely corroborates the unbiased clustering
217 (**Fig. S5**), and the transcriptional profiles of individual T-types are consistent with distinct hDRG
218 neuronal classes previously reported (**Fig. 3C**). In addition, we identified 342 genes that are
219 differentially expressed across T-types (**Table S3**), including 27 physiologically relevant genes
220 (**Fig. 3D**).

221 Patch-seq links E-type 2 to transcriptionally defined C-PEP hDRG neurons

222 Subpopulations of DRG sensory neurons exhibit significant differences in ion channel
223 gene expression, modality-specificity, and conduction velocity(*14*, *16*, *32*, *34*, *44–46*). We next
224 asked whether we can correlate hDRG electrophysiological and transcriptional identities. In total,
225 56 Patch-seq samples passed both electrophysiological and transcriptional analysis QC metrics
226 and thus were assigned both E-types and T-types (**Fig. 4A**). These Patch-seq samples show
227 similar E-type and T-type distributions compared to those of the larger populations examined
228 solely in the electrophysiological or transcriptional analysis (**Fig. 4B,C**), despite the small sample
229 size. When we examined individual T-types, the E-type distributions in A-LTMR, A-PEP, and C-

230 NP neurons are similar to that of all Patch-seq samples when analyzed regardless of their T-types
231 (**Fig. 4D**). Single-spiking, low amplitude E-type 3 is the most abundant in these T-types and
232 constitutes more than half of the A-LTMR (61.9%) and A-PEP (58.3%) subpopulations. However,
233 the C-PEP neurons had a significantly different E-type distribution from the other T-types, with
234 most C-PEP neurons (83.3%) belonging to repetitive-spiking E-type 2, a 2.4-fold increase than
235 other hDRG T-types. This suggests that C-PEP nociceptors are often low threshold, multi-spiking
236 neurons. Consistently, E-type 2 Patch-seq samples exhibit significantly higher expression of
237 hDRG nociceptor markers, such as *TAC1* and *CALCA* (**Fig. 4E, Table S4**), and its DE genes are
238 important for the perception and response to pain (**Fig. 4F**). Taken together, our Patch-seq data
239 suggests that hDRG C-PEP nociceptors are frequently multi-spiking E-type 2 neurons, whereas
240 A-fiber neurons (A-LTMR and A-PEP) are more likely to exhibit high-threshold single-spiking
241 phenotypes (E-types 1, 3).

242 Donor pain history is associated with E-type-specific differences in action potential 243 waveform and intrinsic membrane properties of human somatosensory neurons

244 Persistent nociceptor hyperexcitability in low threshold, multi-spiking DRG neurons is
245 thought to drive persistent pain following nerve injury in rodents (*12*). Human somatosensory
246 neurons resected from cancer patients with radiculo-neuropathic pain exhibit similar
247 hyperexcitability and ectopic activity (*9–11*). However, it is unknown which cell types might
248 underlie this ongoing pain, or whether these findings extend to other pain modalities like low back
249 pain, which is the leading cause of disability worldwide (*47*). Therefore, we tested whether a
250 donor's history of pain was associated with any differences in membrane excitability and kinetics
251 of repetitive and single-firing clusters of small- to medium-diameter hDRG neurons.

252 Donors were classified as having no significant pain history ("No Pain Hx") or having a
253 significant pain history in the dermatome of thoracolumbar DRGs ("Pain Hx") based on the
254 medical history reported by the next of kin (**Table 3, Table S1**). As the organ donors' medical chart
255 was not available through the organ registry paperwork, the medical history reported by the next
256 of kin was used as a proxy. A donor was classified as having significant pain history if they met
257 two out of three of the following criteria: (a) the word "pain" is used to describe donor's recent or
258 present medical condition (e.g., "daily pain," "regular pain," "painful tendonitis"), and the
259 description of pain is aligned to thoracolumbar dermatomes (e.g., low back and/or the lower body);
260 (b) donor's medical history includes prescribed use of analgesics (e.g., hydrocodone or
261 gabapentin) that is unrelated to substance use disorder, or there is documentation of other non-

262 pharmaceutical interventions for pain (e.g., back surgery, nerve blocks); (c) donor's medical
263 history includes a disorder for which pain is a major symptom, such as arthritis or scleroderma. If
264 the donor's reported history was negative for all three criteria, the donor was classified as no
265 significant pain history; donors who met one, but not all, of the criteria above were considered
266 possible confounds and excluded from further analysis.

267 Using the above criteria, we identified 13 donors (23.21%) as having a significant pain
268 history ("Pain Hx"), which is close to the estimated prevalence of chronic pain among adults in
269 the United States (*48*). Thirty-four donors were identified as having no significant pain history ("No
270 Pain Hx"). Nine donors were excluded as possible confounds. The most common locations of
271 pain were knee (5/13 donors) and low back (4/13 donors) pain (**Table 3**). The two most common
272 etiology of pain were musculoskeletal conditions (5/13 donors; osteoarthritis, tendonitis, injury)
273 and issues with intervertebral disks (3/13, "bulging" or "degenerative" disk; **Table 3).** There was
274 no significant difference in the age, body mass index, or relative distributions of race, sex, and
275 cause of death between the Pain Hx and No Pain Hx groups (**Table S5**). This suggests that low
276 back pain and musculoskeletal pain are the most common chronic pain complaints seen in this
277 organ donor group, which is consistent with population-level observations (*47*).

278 A total of 39 patch-clamp recordings in our E-type database were from hDRG neurons of
279 Pain Hx donors. Upon post-hoc analysis, the majority of the recordings (61.54%) were obtained
280 from two pain donors with low back pain (**Table 3**). Both groups had similar proportions of E-types
281 1, 2, and 3 (**Fig. S7**), suggesting that the overall distribution of the E-types does not vary between
282 the two groups.

283 Next, we compared the electrophysiological properties of each E-type between the Pain
284 Hx and No Pain Hx groups. Out of the 39 total patch-clamp recordings obtained from Pain Hx
285 donors, only 4 neurons (10.53%) belonged to E-type 1 (**Fig. S7**), which represents a low-
286 excitability phenotype that appears to map onto the A-LTMR and A-PEP T-types (**Fig. 1, 2**). The
287 membrane properties, spike kinetics, and spike firing pattern of E-type 1 appeared to be largely
288 similar across the two groups with the exception of rheobase, which trended higher in the E-type
289 1 neurons from the Pain Hx group (**Table S6, Fig. S8**). Statistical comparison was limited by the
290 small sample size of E-type 1 in the Pain Hx group.

291 E-type 2 neurons exhibit a highly excitable multi-spiking phenotype (**Fig. 1, 2**) that strongly
292 correlated with the C-PEP T-types and express high levels of human nociceptor markers (**Fig. 4**).
293 The overall AP half-width, rise time, and decay time were not significantly different between the

294 Pain Hx and No Pain Hx groups (**Fig. 5A-D**). However, we found that E-type 2 neurons from Pain
295 Hx group had significantly larger action potential amplitude (**Fig. 5E, F**) and significantly higher
296 voltage sag (**Fig. 5G, H**) compared to the No Pain Hx group. There were no significant differences
297 in the overall spike firing, rheobase, input resistance, or resting membrane potential between the
298 two groups (**Fig. 5I, J; Table S7**).

299 Finally, E-type 3 represents a cluster of hDRG neurons with low excitability and a
300 characteristic narrow, fast action potentials that are biased towards A-PEP and A-LTMR T-types.
301 E-type 3 neurons from Pain Hx group were associated with faster decay and a narrower half-
302 width (**Fig. 5K-N; Table S8**); however, these differences did not meet the adjusted threshold for
303 statistical significance after controlling for multiple comparisons (alpha=0.005, Bonferroni
304 correction). Peak and amplitude were comparable between groups (**Fig. 5O, P; Table S8**). E-type
305 3 neurons in the Pain Hx group also showed trends towards a more depolarized resting
306 membrane potential (**Table S8**) and a larger voltage sag (**Fig. 5Q,R**); however, other intrinsic
307 membrane properties like rheobase, overall spike firing, action potential threshold, and input
308 resistance were similar between the Pain Hx and No Pain Hx groups (**Fig. 5S,T; Table S8**).
309 Together, these findings suggest that history of pain may be associated with E-type-specific
310 differences in action potential kinetics in human somatosensory neurons, with the most
311 pronounced differences seen in E-type 2, a cluster most strongly correlated with human
312 nociceptors.

313 Pain history is associated with higher NaV1.7 and 1.8 expression in human sensory 314 neurons

315 Voltage-gated sodium channels NaV1.7, 1.8, and 1.9 are selectively expressed in the
316 peripheral nervous system, act as key modulators of nociceptor excitability, and are thought to
317 drive neuronal hypersensitivity that underlies persistent pain (*49*, *50*). The genes that encode
318 these channels, *SCN9A* (encodes NaV1.7), *SCN10A* (NaV1.8), and *SCN11A* (NaV1.9), are
319 selectively expressed amongst nociceptor subtypes in mouse, though they appear to be more
320 broadly expressed in both nociceptor and non-nociceptor subpopulations in hDRG (*18*, *51–58*).
321 As the expression of these voltage-gated sodium channels are upregulated in animal models of
322 pain, (*59*) we investigated if there is pain history-associated differences in their expression in
323 hDRG.

324 First, we conducted a preliminary analysis of the expression of *SCN9A*, *SCN10A*, and
325 *SCN11A* using our Patch-seq dataset. After segmenting the dataset by donor's pain history (**Table**

326 **3**), we observed trends towards higher *SCN10A* and *SCN11A* expression (16% and 33%,
327 respectively) in hDRG neurons from donors with pain history (n=16; Pain Hx) compared to hDRG
328 neurons from donors without pain history (n=73; No Pain Hx). However, given the small sample
329 size, we were unable to further segment these results by E-types for differential expression (DE)
330 analysis. Therefore, we opted to use a complementary approach to examining the distribution of
331 *SCN9A*, *SCN10A*, and *SCN11A* expression in our donor population through RNA *in situ*
332 hybridization. We quantified expression level in the DRG in two ways: (1) the overall percentage
333 of DRG neurons that express the target gene, and (2) the relative expression level (e.g., number
334 of mRNA copies of target gene) within each positive neuron. The Pain Hx group trended towards
335 having a larger proportion of hDRG neurons expressing *SCN9A* and *SCN10A* compared to the
336 No Pain Hx group, though the difference was not statistically significant (p=0.0655 and 0.0659,
337 respectively; **Fig. 6A-B, E-F**). However, the expression levels of *SCN9A* and *SCN10A* per cell
338 were significantly higher in the Pain Hx group compared to the No Pain Hx group (**Fig. 5C**, **G**).
339 Increased copy numbers of *SCN9A* and *10A* were observed in small- and medium-sized hDRG
340 neurons (**Fig. 5D, H**). While *SCN11A* expression was also higher in the Pain Hx group compared
341 to the No Pain Hx group, as measured in terms of proportion and within-cell expression (**Fig. 5M-**
342 **P**), this difference was not statistically significant. Interestingly, *SCN9A*, but not *SCN10A* or
343 *SCN11A*, was detected in satellite glial cells surrounding neuronal cell bodies (**Fig. S9**), confirming
344 previous observations (*11*, *42*).

Discussion

In the present study, we found that human sensory neurons exhibit three distinct E-types *in vitro*. Using Patch-seq, we mapped these electrophysiologically-defined E-types to transcriptionally-defined subpopulations of human sensory neurons, or T-types. Our findings indicate that the multi-spiking, high-excitability physiological subtype (E-type 2) is strongly correlated with C-fiber peptidergic (C-PEP) nociceptor subtype of hDRG neurons. Further, our investigation into the donor pain history revealed cluster-specific differences in action potential kinetics in hDRG neurons from donors with and without reported pain history, which may be partially explained by higher expression of *SCN9A* and *SCN10A* in lumbar hDRG of donors with pain history. Together, our work demonstrates how these types of multimodal datasets can be used to link functional phenotypes to different human sensory neuron populations and generate hypothesis-driven investigations into pain pathophysiology.

Physiological heterogeneity of human sensory neurons

Multiple studies in both rodent and human DRG have classified nociceptors based on their electrophysiological features such as spiking patterns, action potential kinetics, presence of hump or shoulder in the rise or decay phase of the action potential, action potential firing latency, or presence of ectopic activity(*9*, *10*, *12*, *13*, *25*, *26*, *60*). In this study, we chose an unbiased clustering method that integrates multiple electrophysiological features. This approach avoids bias that may occur with subjective classification of E-types. This also allowed us to detect subtle differences in AP waveforms that might be influenced by distinct combinations of voltage-gated channels. Additionally, utilizing a large pool of donors for our sample collection allowed us to reduce potential donor bias in the classification process.

Echoing prior studies in rodents(*12*, *25*) and hDRG cultures (*61*), our analysis found that hDRG neurons demonstrate a wide variety of electrophysiological characteristics and evoked action potential firing patterns. In our pool of small diameter hDRG neurons (<60µm), three E-types emerged, with E-type 2 representing a highly excitable, multi-spiking subset a hDRG neurons and E-types 1 and 3 representing two clusters of low excitability neurons. Our control analyses suggest that distribution of E-types is not significantly related to number of days in culture seen under our experimental conditions, suggesting that number of days *in vitro* does not strongly influence E-type of each hDRG neuron between 2-11 days in culture.

It is unknown whether these E-types represent discrete, immutable physiological classes of hDRG neurons, or whether they reflect different possible electrophysiological *states*. Prior

377 studies on spiking patterns provide some insight: for instance, persistent (i.e., 24hr) depolarization
378 or prolonged exposure to inflammatory mediators can lead to changes in relative representation
379 of single or repetitive-firing phenotypes in cultured human and rodent DRG neurons (*60*, *62*). This
380 switch in firing patterns is not seen following acute exposure to inflammatory mediators (e.g.,
381 bradykinin) in hDRG neurons, which imply that spiking pattern changes may only occur in
382 response to strong and persistent stimuli (*13*). While spike pattern is only one of many features
383 that are incorporated in our E-type classification, these past studies suggest that E-types may
384 reflect different functional states of hDRG neurons. This is further supported by our finding that T-
385 types map onto more than one E-type.

386 The idea that E-types reflect functional states rather than a fixed phenotype may appear
387 to be in conflict with our finding that E-type 3 neurons are significantly larger than E-type 2 neurons.
388 However, our patch-seq analysis shows that A-LTMR and A-PEP, two T-types associated with
389 large-diameter hDRG cells, are biased towards E-type 3. Then, it is possible that T-types are
390 biased towards certain E-type at baseline, but that this E-type – or the electrophysiological state
391 – may be plastic (*13*, *60*).

392 Physiological specialization in transcriptionally distinct clusters of human sensory 393 neurons

394 Linking the electrophysiological and transcriptional phenotypes in hDRG poses unique
395 challenges due to the lack of readily available genetic labelling strategies, and the widespread
396 distribution of nociceptors across multiple cell sizes. Patch-seq recordings allowed us to
397 circumvent these challenges and obtain both electrophysiological and transcriptional data from
398 the recorded hDRG neuron.

399 Recordings from genetically labeled mouse lines have revealed markedly different
400 electrophysiological characteristics across DRG cell types (*25*). Each genetically labelled
401 subpopulation of mouse sensory neurons is often associated with one distinct physiological
402 phenotype, with the exception of peptidergic nociceptors which appear to be heterogeneous (*25*).
403 In contrast to the earlier findings in mouse, we observed that hDRG T-types tend to map onto
404 multiple E-types (**Fig. 4**), which suggests that transcriptionally defined subtypes of human sensory
405 neurons are physiologically heterogeneous. Intriguingly, C-PEP – which reflects peptidergic
406 nociceptors, a subpopulation which is thought to be more physiologically heterogeneous than
407 other DRG classes (*25*, *26*) -- was the only T-type that had a significantly different E-type
408 distribution and the only T-type to be predominantly made up of E-type 2, the highly excitable,
409 multi-spiking E-type. Further studies are required to determine whether this is attributable to

410 experimental conditions, such as differences in cell-type resolution between the studies or
411 alterations in cell type marker gene expression *in vitro*, which may confound cell-type annotation
412 in Patch-seq analysis (*63*). Alternatively, this departure from findings in mouse DRG may reflect
413 the much more varied genetics, environments and histories (health status, exposures, injuries) of
414 the human donors compared to inbred rodent lines raised in highly controlled environments.
415 Finally, these differences may represent yet another cross-species difference in somatosensory
416 neurons in addition to the transcriptional and molecular differences that have been characterized
417 (*31*–*37*).

418 As the field continues to define the molecular features that distinguish hDRG cell types, it
419 is possible that a given transcriptional class can include distinct subtypes based on their
420 physiological or anatomical properties. While determining the axonal projections of defined DRG
421 cell types will be a major hurdle in humans, information about soma diameter or axonal branching
422 *in vitro* is readily available and may help to further distinguish specific cell types(*34*, *38*). In this
423 study, we focused on smaller diameter neurons that are more likely to be nociceptors(*34*) and this
424 approach can be expanded to study other cell types within the hDRG. In future studies, it will be
425 valuable to incorporate different physiological stimuli, like temperature or pressure, to further
426 characterize the response properties of specific populations of human sensory neurons.
427 Continued investigation into the link between physiological characteristics and transcriptional
428 features may, in the future, allow researchers to more reliably predict the transcriptional phenotype
429 of a hDRG neuron based solely on physiological properties: for instance, neurons from different
430 T-types that show similar firing patterns (i.e., E-type 2 neurons from A-PEP vs. C-PEP clusters)
431 may have subtle electrophysiological differences that could be revealed with large collaborative
432 efforts across the field. We suggest that multimodal approaches combining molecular profiling
433 through single-cell sequencing or qPCR with recordings from human sensory neurons will be an
434 essential step to fully understand the cell type diversity of human DRG. This may also present an
435 opportunity to more directly relate new observations in human tissue to the decades of knowledge
436 about the underlying neurobiology of pain and somatosensation developed using more tractable
437 animal models.

438 Rapid advancements in high-throughput technologies to profile human tissue at cellular
439 resolution have led to the identification of increasingly nuanced cell types. The biological ground
440 truth of what defines a cell type is likely to require multimodal profiling across healthy and disease
441 states. Previously, Patch-seq recordings have been used in rodent sensory neurons to identify
442 mechanisms of mechanosensitivity (*40*) and human pluripotent stem cell-derived sensory neuron

443 cultures (*64*). Developing a clearer picture of the features that define native human neurons will
444 be useful to guide reprogramming efforts to better model and understand human disease using
445 patient cells. Moreover, excitability changes within molecularly defined cell types could be used
446 to identify different neuronal populations that could be drivers of specific chronic pain conditions,
447 and potential therapeutic targets selectively expressed within those affected neurons. This will
448 require harmonized datasets across large numbers of donors to fully realize this potential.

449 The data presented here represent an interim analysis of a planned larger effort to
450 generate a large multimodal database of hDRG neurons that will eventually be used to compare
451 sensory neuron characteristics within and across species. The dataset may provide additional
452 predictive value to preclinical studies using cultured DRG neurons, as it may allow prediction of
453 transcriptional/functional phenotype based on physiological markers. This type of detailed
454 analysis of E-type relative to T-type represents a long-term goal of our NIH HEAL Initiative-
455 supported human tissue program (part of the PRECISION Human Pain Network) and will require
456 hundreds of recordings collected over several years to know whether specific electrophysiological
457 features of hDRG neurons can be used exclusively to identify the recorded cell type. At present,
458 we suggest that adding Patch-seq to recordings from human sensory neurons affords the
459 opportunity to analyze physiological differences in genetically defined subsets of sensory neurons,
460 reducing the impact of cell type heterogeneity and allowing for more direct comparisons of human
461 sensory neuron biology to the cell-type-specific data collected from animal model studies.

462 Pain-associated differences in neuronal excitability

463 To date, several electrophysiological analyses of dissociated hDRG neurons have been
464 completed using samples obtained from cancer patients with neuropathic pain (*9–11*). Here, we
465 aimed to use our dataset to see similar analyses could be conducted in samples obtained from
466 organ donors.

467 Our study highlights both strengths and weaknesses of the approach of hDRG from organ
468 donors for the study of somatosensation. In contrast to studies utilizing animal tissue, it is
469 impossible to control for the entirety of a donor's lived experience and there are likely many gaps
470 in available medical histories. Therefore, it is possible that there could be chronic pain diagnoses
471 or pain symptoms that were not reported. Our dataset almost certainly contains neurons that do
472 not innervate the dermatome of pain in our pain donors. As a result, some of the heterogeneity
473 seen in our Pain Donor dataset may be reflective of the heterogeneity in the innervation pattern
474 of recorded neurons. Traditionally, innervation patterns of rodent DRG neurons have been
475 identified through techniques such as genetic labeling and tracer injections which cannot be used

476 in human subjects. However, as we develop increasingly more detailed understanding of hDRG
477 gene expression patterns, we can utilize techniques like multiplexed immunohistochemistry
478 techniques in various peripheral tissues such as skin and visceral organs to make predictions
479 about the innervation patterns of hDRG subpopulations.=These are all inherent challenges in
480 human-based research and will require the collective efforts of the pain research community to
481 overcome.

482 Despite these limitations, the use of hDRG from organ donors allows us to more closely
483 sample the chronic pain population at large. The prevalence of pain history in our donor pool was
484 consistent with the estimated prevalence of chronic pain amongst adults in the U.S., and the pain
485 history and location of chronic pain were consistent with the most common etiologies of chronic
486 pain that is seen at a population level. For the present analysis, we included only donors with
487 musculoskeletal pain conditions, but with continued efforts to build these data sets, eventually
488 one can create more refined subcategories (e.g. only low back pain, which may have different
489 drivers and involve different sensory neuron subtypes than arthritis, for example). While our
490 analysis focused on pain history, our approach can be applied toward hypothesis-driven
491 investigation based on other aspects of donor histories, such as substance use. One way to
492 address the issue of heterogeneity is through a large sample size; a collaborative network of
493 multiple labs and institutions with access to human tissue that can work together to contribute to
494 a large, open database of hDRG neuronal recordings.

495 In our analysis, segmentation by pain history revealed E-type-specific differences in
496 physiological features. The largest difference between groups was seen in E-type 2 neurons,
497 which had significantly higher action potential peaks and larger amplitude. Action potential
498 amplitude and peak are predominantly determined by voltage-gated sodium currents. In
499 somatosensory neurons, NaV1.8 is the main determinant of the action potential amplitude: it
500 contributes a large proportion of depolarizing currents during the rising phase of the action
501 potential and has relatively depolarized steady-state inactivation, enabling robust spike
502 amplitudes even at depolarized membrane potentials (*65*). Additionally, NaV1.7 may indirectly
503 modulate the amplitude and peak by lowering the voltage threshold. The greater within-cell
504 expression of *SCN9A* and *SCN10A* in the Pain Hx group suggest that upregulation of these two
505 channels may underly some of the amplitude and peak differences seen in the Pain Hx group.
506 Given that we did not see any differences in action potential threshold between the Pain Hx and
507 No Pain Hx groups, NaV1.8 likely has a bigger contribution to the larger action potential height
508 seen in the E-type 2 neurons of the Pain Hx group. In addition to the spike amplitude, Pain Hx

509 was also associated with a larger voltage sag in E-type 2. While not statistically significant, E-type
510 3 neurons also showed similar trends towards larger voltage sag in the Pain Hx group. Voltage
511 sag is primarily driven by hyperpolarization-activated cyclic nucleotide-gated (HCN) channels,
512 which in turn can be modulated by cAMP signaling. Possible mechanisms that may underly the
513 increased voltage sag seen in E-type 2 neurons from Pain hx donors include upregulation of HCN
514 channel expression and potentiation of HCN-mediated current (I_h) (*66*–*68*) due to altered GPCR
515 tone. Since G protein pathways regulate numerous other ion channel and receptor families,
516 including voltage-gated sodium channels, it will be important to directly compare expression and
517 function between donor populations in future studies.

518 Our RNA *in situ* hybridization results point towards increased expression of NaV1.7 and
519 1.8 in hDRG obtained from pain donors. Unlike animal studies which enable greater experimental
520 control which can provide more definitive conclusions about the directionality in the relationship
521 between injury and ion channel expression, we are not able to draw causative conclusions due to
522 the observational, rather than experimental, nature of our study involving donor-obtained hDRG
523 neurons. However, a wealth of studies in animal models demonstrates that upregulation of
524 NaV1.7 and 1.8 following injury or insult underlies the pathogenesis of persistent pain across
525 multiple animal models (*11*, *69*–*72*). It is also possible that donors with Pain Hx had high levels
526 of NaV1.7 and 1.8 at baseline, and that this predisposed them to developing chronic pain, as are
527 seen in individuals born with gain-of-function mutations in NaV1.7 or 1.8 that predispose them to
528 developing hereditary small-fiber neuropathies (*73*–*76*). The association between increased
529 *SCN10A* expression and pain history is particularly intriguing considering the recent FDA-
530 approval of the NaV1.8 inhibitor, suzetrigine (VX-548), which reduces post-surgical pain
531 compared to placebo, with comparable efficacy to hydrocodone/acetaminophen (*77*, *78*).

532 In summary, our study identifies three distinct electrophysiological phenotypes of human
533 somatosensory neurons, which can be linked to specific transcriptionally defined subpopulations
534 using Patch-seq. Highly excitable E-type 2 appears to be strongly associated with the C-fiber
535 peptidergic subpopulation of hDRG neurons. We additionally demonstrate that pain history is
536 associated with E-type-specific differences in membrane properties and action potential amplitude,
537 which may be due to higher levels of NaV1.7 and 1.8 expression. Detailed knowledge into how
538 the properties of native human neurons are altered in chronic pain conditions may reveal new
539 insights that can inform specific therapeutic strategies tailored to distinct etiologies of pain.

Acknowledgements

We thank the past and present members of the Gereau lab for their helpful comments, and Mid-America Transplant for their collaboration in donor screening and tissue procurement. Finally, we thank the organ donors and their families, whose invaluable gift made this research possible.

This work was supported by the American Heart Association (AHA) through the AHA Predoctoral Fellowship #828671 (JY) and by the National Institutes of Health (NIH) through the NIH HEAL Initiative under award number U19NS130607 (RWG, BAC), part of the NIH PRECISION Human Pain Network. We thank the Genome Technology Access Center at McDonnell Genome Institute at Washington University School of Medicine for help with sequencing and data processing for the Patch-seq experiment. The Center is partially supported by NCI Cancer Center Support Grant #P30 CA91842 to the Siteman Cancer Center from the National Center for Research Resources (NCRR), a component of the National Institutes of Health (NIH), and NIH Roadmap for Medical Research.

Funding

American Heart Association Pre-Doctoral Fellowship 828671 (JY)

National Institutes of Health grant U19NS130607 (RWG, BAC)

Author contributions

Conceptualization: JY, BAC, RWG

Data Curation: JY, LY, AC, KK

Formal Analysis: JY, LY, KK

Funding Acquisition: BAC, RWG

Investigation: JY, LY, AJW, AT, ZB, JDR, RAS, MP, AJD, JNL, RK, PG, JMM, GM, JL

Methodology: JY, LY, AJW, RWG, BAC

Visualization: JY, LY

Supervision: BAC, RWG

Writing—original draft: JY, LY

Writing—review & editing: JY, LY, BAC, RWG, AJW, ZB, JDR, RAS, AJD, JNL, RK, PG, AC

Competing interests

Authors declare that they have no competing interests.

571 ## Data availability

572 Donor metadata and electrophysiology data will be made available upon publication as an
573 open repository via the SPARC Data Portal (doi.org/10.26275/thj5-bs3v) as approved by the NIH
574 Data Coordination and Integration Center. Single-cell RNA sequencing data will be made
575 available upon publication on dbGaP (accession number phs003788.v1.p1). Other data pertaining
576 to this study will be made available upon reasonable request.

Methods

hDRG extraction

Extraction and collection of hDRGs were performed as previously described(*79*) in collaboration with Mid-American Transplant, with the following modifications and specifications. T11 - L5 DRGs were surgically removed from postmortem organ donors, within 1 -3 hours of aortic cross-clamping. Extracted DRGs were immediately placed in ice-cold, oxygenated N-methyl-D-glucamine (NMDG)-based artificial cerebrospinal fluid (aCSF; 93 mM NMDG, 2.5 mM KCl, 1.25 mM NaH_2PO_4, 30 mM $NaHCO_3$, 20 mM HEPES, 25 mM glucose, 5 mM ascorbic acid, 2 mM thiourea, 3 mM Na^+ pyruvate, 10 mM $MgSO_4$, 0.5 mM $CaCl_2$, 12 mM N-acetylcysteine; adjusted to pH 7.3 using NMDG or HCl, and 300 - 310mOsm using H_2O or sucrose) and transported to lab for processing.

Donor inclusion and classification

Donors that were older than 60 years, had a body mass index greater than 40, or had positive serology for blood-borne diseases such as hepatitis C or human immunodeficiency virus (HIV) were excluded from the study. Donor's past medical history was determined using available information on the United Network of Organ Sharing (UNOS) documentation and interviews conducted by Mid-America Transplant with family members. A donor was classified as having significant pain history if they met two out of three of the following criteria: (a) the word "pain" is used to describe donor's recent or present medical condition (e.g., "daily pain," "regular pain," "painful tendonitis,"), and the dermatome of pain is specified to be in the back and/or the lower body; (b) donor's reported history includes prescribed use of analgesics (e.g., hydrocodone or gabapentin) that is unrelated to substance use disorder, or there is documentation of other non-pharmaceutical interventions for pain (e.g., back surgery, nerve blocks); (c) donor's reportedhistory includes a disorder for which pain is a major symptom, such as arthritis or scleroderma. Based on these inclusion criteria, eight donors were identified as having a significant pain history ("Pain Hx"). Donors whose reported medical history did not mention any significant or possible pain conditions were classified as having no pain history ("No Pain Hx"). Finally, donors who only partially met the above criteria or had medical histories that included descriptions of possible pain-related conditions but lacked sufficient details to positively determine their pain statuses were considered to be possible confounds and excluded from further segmentation by pain history Demographic information and pain-related history of each donor is provided in **Table 1** and **Table S1**.

609 ## hDRG primary culture

610 Primary culture of hDRGs were performed as previously described(*60*, *79*). Briefly, 2 - 3
611 thoracolumbar DRGs were cleaned and finely minced using ice-cold NMDG-aCSF. Minced DRGs
612 were sequentially dissociated using papain (Worthington, Lakewood NJ) and collagenase type 2
613 (Sigma-Aldrich, Darmstadt, Germany), then triturated for mechanical dissociation. Dissociated
614 DRGs were filtered and resuspended in DRG media (5% fetal bovine serum [Gibco, Grand Island,
615 NY], 1% penicillin/streptomycin [Corning, Corning, NY], Glutamax [Life Technologies, Carlsbad,
616 CA), and B27 [Gibco] in Neurobasal-A [Gibco]). DRG were plated and cultured on PDL and
617 collagen-coated glass coverslips, and media was changed every 2 - 3 days.

618 ## Patch-clamp electrophysiology

619 Patch-clamp experiments were performed between days in vitro (DIV) 2 - 11. Current
620 clamp experiments were performed in external solution containing (in mM): 145 NaCl, 3 KCl, 2
621 $CaCl_2$, 1 $MgCl_2$, 7 glucose, 10 HEPES, adjusted to pH 7.3 with NaOH. Patch pipettes were pulled
622 from thin-walled borosilicate glass with outer diameter of 1.5mm and internal diameter of 1.10mm
623 (Sutter Instruments, Novato, CA). Pipettes were fire polished and had resistance values of 1 - 4
624 MΩ. The internal solution consisted of the following (in mM): 120 K-gluconate, 5 NaCl, 3 $MgCl_2$,
625 0.1 $CaCl_2$, 10 HEPES, 1.1 EGTA, 4 Na_2ATP, 0.4 Na_2GTP, 15 Na_2Phosphocreatine; adjusted to pH
626 7.3 with KOH and HCl, and 290 mOsm with sucrose. Patch-seq experiments were conducted with
627 a modified K-gluconate internal designed to promote cDNA yield while maintaining
628 electrophysiological properties, containing the following: 110 K-gluconate, 4 NaCl, 10 HEPES, 0.2
629 EGTA, 1 Na_2ATP, 0.3 Na_2GTP, 10 Na_2Phosphocreatine, 20 µg/mL glycogen, and 0.25 µL Protector
630 RNAse Inhibitor; adjusted to pH 7.3 with KOH and HCl, and 290 mOsm with sucrose. Experiments
631 were performed at room temperature. External solution was perfused continuously at a rate of 1
632 - 2 mL/min using a gravity-fed bath perfusion system. Recordings were made using a MultiClamp
633 700B amplifier, a Digidata 1550B digitizer, and the pClamp software (v.11.1, Molecular Devices,
634 San Jose, CA). All recordings were sampled at 10 kHz.

635 hDRG neurons with soma diameter <60 µm were preferentially patched to increase the
636 likelihood of recording from nociceptor populations(*34*). Membrane properties and excitability
637 were measured in current clamp mode. After a stable whole-cell configuration was achieved and
638 maintained for at least 2 minutes, a gap-free current-clamp recording was carried out for 1 - 2
639 minutes with zero current injection in order to assess resting membrane potential and
640 spontaneous activity. After the resting membrane potential was measured, hDRG neurons were
641 held at -60 mV for assessment of membrane excitability and passive properties. Membrane

642 excitability was determined using 1-s long stepwise current injections starting at 50 pA (Δ 50 pA)
643 until at least one action potential spike was elicited. To determine spiking pattern, suprathreshold
644 currents at 1-, 2-, 3-, and 4-fold rheobase were injected using the same 1-s long stepwise protocol.
645 hDRG neurons that had an unstable resting membrane potential, were depolarized >30mV at rest,
646 or required more than -500pA to be held at -60mV were considered to be unhealthy and
647 recordings from those cells were excluded from analysis for quality control.

648 Analysis of excitability, spike kinetics, and membrane properties was conducted using
649 Easy Electrophysiology (Easy Electrophysiology Ltd., London, UK) and an in-house pipeline for
650 automated analysis of electrophysiological data using the criteria described below. Rheobase was
651 defined as the minimum current injection required to trigger an action potential firing. To assess
652 spike firing pattern, the number of action potential spikes fired in response to each current step
653 was counted to generate an input-output curve for each cell. The action potential threshold was
654 defined as the membrane voltage when the first derivative of the voltage crossed 10 mV/ms (dV/dt
655 = 10) and was determined from the first action potential fired at rheobase. Action potential kinetics
656 were measured using the first action potential fired at rheobase. Maximum rise and decay times
657 were obtained from 10 - 90% of the rising and falling phases, respectively. Action potential half-
658 width was defined as the time between 50% of the rising and falling phases. Action potential
659 amplitude was measured from action potential threshold to the peak of the spike, and peak was
660 measured from 0mV to the peak of the spike. Input resistance was measured using
661 hyperpolarizing current injections from -250 pA to -50 pA (Δ50 pA), by plotting ΔV_m against ΔI and
662 determining the slope of the line of best fit. Voltage sag was measured using a single -250pA
663 hyperpolarizing step. The magnitude of the sag was calculated as the difference between peak
664 deflection and the steady-state V_m. The sag ratio was calculated by dividing the sag by the peak
665 deflection magnitude.

666 Cytosol extraction for RNA-seq

667 After the conclusion of whole-cell recording, cytosolic contents were aspirated into the
668 recording pipet using gentle negative pressure for 2 - 3 minutes, until a visible shrinkage of the
669 cell was observed (Fig. S5A). After aspiration, the recording pipette was slowly and gradually
670 withdrawn. Contents of the patch pipette were immediately ejected into a sample collection tube
671 containing 1 µL 10 x Reaction Buffer (95% Lysis Buffer [Takara Bio] and 5% RNAse inhibitor
672 [Takara Bio]) and 8µL RT-PCR grade nuclease-free water (Thermo Scientific) by applying
673 positive pressure. Samples made of Patch-seq internal solution were used as negative controls
674 to assess ambient RNA contamination. Samples were stored at -80 °C for long-term storage.

675 For Patch-seq experiments, experimenters were agnostic to the pain history status of the
676 donors.

677 ## RNA sequencing and quality control of cytosolic contents

678 RNA was converted into cDNA using SMART-Seq v4 Ultra Low Input RNA Kit for
679 Sequencing following the manufacturer's manual. Samples containing 50 pg of total mouse brain
680 RNA and samples made of nuclease-free water were used as positive and negative controls for
681 library preparation, respectively. Twenty PCR cycles were used for cDNA amplification to increase
682 yield. cDNAs were assayed using an Agilent TapeStation 4200. Samples were deemed high
683 quality and proceed with sequencing library preparation if they met the following criteria: 1).
684 containing no less than 1 ng of total cDNA, 2) at least 30% of total cDNA falling in the size range
685 of 500 – 6000 bp, and 3). Both cDNA yield and cDNA percentage in range metrics were at least
686 25% higher than its associated negative controls.

687 The cDNA libraries that passed quality control were then prepared for sequencing using
688 the Illumina Nextera XT Library Preparation Kit following the manufacturer's manual. Resulting
689 libraries were pooled and sequenced on an Illumina NovaSeq 6000 or NovaSeq X Plus instrument
690 targeting at least 500k reads per library. Sequencing reads were aligned to hg38 Reference
691 genome with STAR version 2.7.9a1. Gene counts were derived from the number of uniquely
692 aligned unambiguous reads by Subread:featureCount version 2.0.32. Sequencing samples with
693 at least 100k reads detected and at least 80% reads mapped to genome were included in the
694 following analysis.

695 ## Transcriptional clustering and T-type annotation of Patch-seq samples

696 In total, 139 samples that passed the cDNA and sequencing quality controls were included.
697 First, the counts table of Patch-seq samples was loaded into Seurat (V4.4.0) in R (V4.4.1) for
698 quality control and gene expression analysis (*80*). Raw counts were scaled to 10,000 transcripts
699 per nucleus using NormalizeData() and scaled for each gene using ScaleData() functions. Highly
700 variable genes were identified, and the top 20 principal components (PCs) were retrieved with
701 RunPCA() using default parameters. Uniform Manifold Approximation and Projection (UMAP)
702 coordinates were calculated using RunUMAP(). Clustering analysis was performed using
703 FindClusters() based on the variable features from the top 10 principal components, with the
704 resolution set at 1.2, and the marker genes for each cluster was identified using FindAllMarkers()
705 comparing cells in one cluster to all other cells. Cell class markers were identified from single-
706 soma RNA-seq data and used for annotating the transcriptional classes in Patch-seq data.

707 Specifically, *SNAP25* and *APOE* were used to identify neuronal clusters and clusters with possible
708 glial gene contamination, respectively. For neuronal classes, clusters with high expression level
709 *CALCA* were identified as peptidergic neurons, and transcription factors, including *NTRK3*,
710 *NTRK1*, and *PRDM12*, were used to identify A-LTMR, A-PEP/C-PEP, and C-NP/C-PEP neurons,
711 respectively (*33*, *37*).

712 To increase cell type resolution, we directly compared the Patch-seq samples from
713 neuronal clusters to single-soma RNA-seq data. First, FindTransferAnchors() was used to identify
714 shared anchors (conserved features) between the datasets. T-type annotation was done using
715 TransferData() that transferred the cell class labels (A-LTMR, A-PEP, C-NP, and C-PEP)
716 described in the published dataset to each Patch-seq cell in the neuronal clusters.

717 Differential expression (DE) analysis

718 DE analysis across T-types or E-types was done using DESeq2 wrapper function in Seurat
719 comparing the gene expression of one group of cells to all other cells. Currently, the DE analysis
720 is underpowered due to small sample size (126 sequenced samples, which were assigned to
721 neuronal clusters were used for T-type DE analysis, samples with glial contamination were
722 excluded, and 56 sequenced sample with E-type annotations for E-type DE analysis), and thus
723 genes with average expression (Log2CPM) > 0.2 and adjusted p value < 0.1 were reported.

724 Gene module scores

725 Gene module scores were calculated for each Patch-seq sample using AddModuleScore()
726 in Seurat. To calculate the neuronal and non-neuronal module scores, DE analysis was performed
727 comparing neuronal and non-neuronal cells from the hDRG cell atlases previously described (*37*).
728 Top 200 marker genes based on Log2FC of neuronal and non-neuronal cells were selected. To
729 calculate the injury scores, DE analysis was performed comparing the hATF3 cells to other cell
730 types from the hDRG single-soma RNA-seq data previously described (*33*). Top 200 marker
731 genes based on Log2FC were selected.

732 Gene ontology (GO) analysis

733 GO analysis was performed using topGO (V2.40.0) in R. Differentially expressed genes
734 described above were used as the input gene list and all genes with average expression >0.5 in
735 the same cells are used as the background gene list. Genes were annotated for their biological
736 process and GO terms with adjusted p value <0.05 were reported.

737 ## *In situ* hybridization

738 L1-L5 hDRGs were fixed in 4% paraformaldehyde at 4 °C overnight, cryopreserved in 30%
739 sucrose, then flash-frozen in OCT. Fixed-frozen hDRG were cryosectioned at 12 µm and mounted
740 on Superfrost Plus slides (Fisher, Pittsburgh, PA). Slides were stored at -20 °C or -80 °C with
741 desiccant until further use. Immediately prior to beginning the *in situ* hybridization protocol
742 (RNAScope, Bio-techne), hDRG sections were dehydrated using 50%, 70%, and 100% ethanol
743 and treated with Protease IV and hydrogen peroxide (ACDBio, Minneapolis, MN). RNAscope was
744 performed following manufacturer's protocol. The following probes from ACDBio were used:
745 SCN9A (cat. no.562251), SCN10A (cat. no.406291), and SCN11A (cat. no.404791). For each
746 experiment, the probe was paired to Opal 570 (1:1000; Akoya Biosciences, Marlborough, MA). To
747 reduce autofluorescence, TrueBlack Autofluorescence Quencher (Biotium, Fremont, CA) was
748 applied at the end of RNAScope following manufacturer protocol, either before or after the
749 application of DAPI. Slides were mounted with coverslips using ProLong Gold Antifade Mountant
750 (Invitrogen, Waltham, MA) and stored at -20 °C until imaging.

751 ## Imaging and image analysis

752 RNAScope slides were imaged using Leica DM6b system at 20 x magnification. For each
753 slide, the entire hDRG section was imaged using the tile scan and merge feature of the using
754 Leica Application Suite X (LAS-X, v.3.7, Leica Microsystems, Wetzlar, Germany). Acquisition
755 settings were kept consistent across all slides and different experimental days. The following
756 acquisition parameters were used: DAPI, 50 ms exposure, 2.1 gain, FIM 30%; L5, 300 ms
757 exposure, 2.5 gain, FIM 55%; TXR, 500 ms exposure, 3.0 gain, FIM 55%. Segmentation and RNA
758 expression analysis was completed using HALO AI™ and the Multiple IHC module of HALO®
759 (Indica labs). Satellite glial cells were distinguished from neuronal cell bodies visually based on
760 their unique morphology.

761 ## Statistics

762 All data were analyzed using GraphPad Prism 10 (GraphPad Software Inc, Boston, MA)
763 and R (V4.4.1). To inform the use of appropriate statistical tests, normality of residuals and
764 heteroscedasticity were assessed for each dataset using Shapiro-Wilk test and Brown-Forsythe
765 test, respectively. To assess statistical differences across multiple groups, one-way ANOVAs with
766 Tukey's post-hoc test, Kruskall-Willis test with Dunn's post-hoc test, or Brown-Forsythe ANOVA
767 with Dunnett's T3 tests were performed. For comparison of multiple electrophysiological features
768 within the same set of samples, Bonferroni correction was applied to determine a multiple

769 comparison-adjusted threshold (α=0.005) for statistical significance. All post-hoc tests were
770 performed with multiple comparison corrections. To assess differences between groups in the
771 input-output curves, restricted maximum likelihood (REML) mixed effects analysis with Geisser-
772 Greenhouse correction was used with Tukey's or Šidák's multiple comparison tests for post-hoc
773 analysis where appropriate. PCA analysis and K-means clustering of electrophysiological data
774 was conducted using R. All data are represented as mean ± SEM unless otherwise noted.
775 Detailed statistics for all comparisons presented in the study can be found in **Supplementary**
776 **Table S9**.

777 Study approval

778 Extraction procedures were approved by Mid-America Transplant, and an Internal Review
779 Board (IRB) waiver was obtained from the Human Research Protection Office at Washington
780 University in St. Louis. hDRG samples were obtained from postmortem organ donors with the
781 consent for tissue donation for research from family members.

References

1. O. Gureje, M. Von Korff, L. Kola, K. Demyttenaere, Y. He, J. Posada-Villa, J. P. Lepine, M. C. Angermeyer, D. Levinson, G. de Girolamo, N. Iwata, A. Karam, G. Luiz Guimaraes Borges, R. de Graaf, M. O. Browne, D. J. Stein, J. M. Haro, E. J. Bromet, R. C. Kessler, J. Alonso, The relation between multiple pains and mental disorders: Results from the World Mental Health Surveys. *Pain* **135**, 82–91 (2008).

2. S. M. Rikard, A. E. Strahan, K. M. Schmit, G. P. Guy, Chronic Pain Among Adults — United States, 2019–2021. *MMWR Morb. Mortal. Wkly. Rep.* **72**, 379–385 (2023).

3. A. Fayaz, P. Croft, R. M. Langford, L. J. Donaldson, G. T. Jones, Prevalence of chronic pain in the UK: A systematic review and meta-analysis of population studies. *BMJ Open* **6**, e010364 (2016).

4. M. L. Ferreira, K. de Luca, L. M. Haile, J. D. Steinmetz, G. T. Culbreth, M. Cross, J. A. Kopec, P. H. Ferreira, F. M. Blyth, R. Buchbinder, J. Hartvigsen, A.-M. Wu, S. Safiri, A. D. Woolf, G. S. Collins, K. Liane Ong, S. Emil Vollset, A. E. Smith, J. A. Cruz, K. Glenn Fukutaki, S. Mekonnen Abate, M. Abbasifard, M. Abbasi-Kangevari, Z. Abbasi-Kangevari, A. Abdelalim, A. Abedi, H. Abidi, Q. Estiningtyas Sakilah Adnani, A. Ahmadi, R. Olusola Akinyemi, A. Tadesse Alamer, A. Zeleke Alem, Y. Alimohamadi, M. Abdullah Alshehri, M. Mansour Alshehri, H. Alzahrani, S. Amini, S. Amiri, H. Amu, C. Liliana Andrei, T. Andrei, B. Antony, J. Arabloo, J. Arulappan, A. Arumugam, T. Ashraf, S. Shamsadin Athari, N. Awoke, S. Azadnajafabad, T. Winfried BÃ, L. H. Barrero, A. Barrow, A. Barzegar, L. M. Bearne, I. M. Bensenor, A. Yirga Berhie, B. Bhandari Bhandari, V. S. Bhojaraja, A. Bijani, B. Boda Abule Bodicha, S. Rao Bolla, J. Brazo-Sayavera, A. M. Briggs, C. Cao, P. Charalampous, V. Kumar Chattu, F. M. Cicuttini, B. Clarsen, S. Cuschieri, O. Dadras, X. Dai, L. Dandona, R. Dandona, A. Dehghan, T. G. Gezahegn Demie, E. Denova-GutiÃ, S. Masudur Rahman Dewan, S. Dhamminda Dharmaratne, M. Lamichhane Dhimal, M. Dhimal, D. Diaz, M. Didehdar, L. Ena Digesa, M. Diress, H. Thi Do, L. Phuong Doan, M. Ekholuenetale, M. Elhadi, S. Eskandarieh, S. Faghani, J. Fares, A. Fatehizadeh, G. Fetensa, I. Filip, F. Fischer, R. Charles Franklin, B. Ganesan, B. Negese Belete Gemeda, M. Erena Getachew, A. Ghashghaee, T. K. Gill, M. Golechha, P. Goleij, B. Gupta, N. Hafezi-Nejad, A. Haj-Mirzaian, P. Kumar Hamal, A. Hanif, N. I. Harlianto, H. Hasani, S. I. Hay, J. J. Hebert, G. Heidari, M. Heidari, R. Heidari-Soureshjani, M. Mbuzeleni Hlongwa, M.-S. Hosseini, A. Kevin Hsiao, I. Iavicoli, S. Emmanuel Ibitoye, I. M. Ilic, M. D. Ilic, S. Mohammed Shariful Islam, M. Dilipkumar Janodia, R. Prakash Jha, H. Ashish Jindal, J. B. Jonas, G. Guyasa Kabito, H. Kandel, R. Jeet Kaur, V. Ranjan Keshri, Y. Saleh Khader, E. Ahmad Khan, M. Jobair Khan, M. A. Khan, H. Reza Khayat Kashani, J. Khubchandani, Y. Jin Kim, A. Kisa, J. KlugarovÃ, A.-A. Kolahi, H. Reza Koohestani, A. Koyanagi, G. Anil Kumar, N. Kumar, T. Lallukka, S. Lasrado, W.-C. Lee, Y. Han Lee, A. Mahmoodpoor, J. N. MalagÃ, M.-R. Malekpour, R. Malekzadeh, N. Malih, M. Mohan Mehndiratta, E. Mehrabi Nasab, R. G. Menezes, A.-F. A. Mentis, M. Kamal Mesregah, T. R. Miller, M. Mirza-Aghazadeh-Attari, M. Mobarakabadi, Y. Mohammad, E. Mohammadi, S. Mohammed, A. H. Mokdad, S. Momtazmanesh, L. Monasta, M. Ali Moni, E. Mostafavi, C. J. L Murray, T. Sadasivan Nair, J. Nazari, S. Aria Nejadghaderi, S. Neupane, S. Neupane Kandel, C. Tat Nguyen, A. Nowroozi, H. Okati-Aliabad, E. Omer, A. Oulhaj, M. O. Owolabi, S. Panda-Jonas, A. Pandey, E.-K. Park, S. Pawar, P. Pedersini, J. Pereira, M. F. P Peres, I.-R.

Petcu, M. Pourahmadi, A. Radfar, S. Rahimi-Dehgolan, V. Rahimi-Movaghar, M. Rahman, A. Masoud Rahmani, N. Rajai, C. R. Rao, V. Rashedi, M.-M. Rashidi, Z. Ahmed Ratan, D. Laith Rawaf, S. Rawaf, A. M. N Renzaho, N. Rezaei, Z. Rezaei, L. Roever, G. de Andrade Ruela, B. Saddik, A. Sahebkar, S. Salehi, F. Sanmarchi, S. G. Sepanlou, S. Shahabi, S. Shahrokhi, E. Shaker, M. Shamsi, M. Shannawaz, S. Sharma, M. Shaygan, R. Ali Sheikhi, J. K. Shetty, R. Shiri, S. Shivalli, P. Shobeiri, M. Mekonnen Sibhat, A. Singh, J. A. Singh, H. Slater, M. Solmi, R. Somayaji, K.-K. Tan, R. Thapar, S. Abolfazl Tohidast, S. Valadan Tahbaz, R. Valizadeh, T. Juhani Vasankari, N. Venketasubramanian, V. Vlassov, B. Vo, Y.-P. Wang, T. Wiangkham, L. Yadav, A. Yadollahpour, S. Hossein Yahyazadeh Jabbari, L. Yang, F. Yazdanpanah, N. Yonemoto, M. Z. Younis, I. Zare, A. Zarrintan, M. Zoladl, T. Vos, L. M. March, L. Back Pain Collaborators, Global, regional, and national burden of low back pain, 1990–2020, its attributable risk factors, and projections to 2050: a systematic analysis of the Global Burden of Disease Study 2021. *Lancet Rheumatol.* **5**, e316–e329 (2023).

5. S. Dey, B. M. Vrooman, Alternatives to Opioids for Managing Pain. *StatPearls* (2022).

6. B. A. Copits, M. Curatolo, P. M. Dougherty, R. W. Gereau, W. Luo, M. Martone, H. Olausson, T. J. Price, W. Renthal, C. J. Woolf, G. Zhao, Human pain neuroscience and the next generation of pain therapeutics. *Neuron* **113**, 1304 (2025).

7. E. T. Walters, R. J. Crook, G. G. Neely, T. J. Price, E. S. J. Smith, Persistent nociceptor hyperactivity as a painful evolutionary adaptation. *Trends Neurosci.*, 1–17 (2023).

8. M. Costigan, J. Scholz, C. J. Woolf, Neuropathic Pain: A Maladaptive Response of the Nervous System to Damage. *Annu. Rev. Neurosci.* **32**, 1–32 (2009).

9. R. Y. North, Y. Li, P. Ray, L. D. Rhines, C. E. Tatsui, G. Rao, C. A. Johansson, H. Zhang, Y. H. Kim, B. Zhang, G. Dussor, T. H. Kim, T. J. Price, P. M. Dougherty, Electrophysiological and transcriptomic correlates of neuropathic pain in human dorsal root ganglion neurons. *Brain* **142**, 1215–1226 (2019).

10. R. Y. North, M. A. Odem, Y. Li, C. E. Tatsui, R. M. Cassidy, P. M. Dougherty, E. T. Walters, Electrophysiological Alterations Driving Pain-Associated Spontaneous Activity in Human Sensory Neuron Somata Parallel Alterations Described in Spontaneously Active Rodent Nociceptors. *Journal of Pain* **23**, 1343–1357 (2022).

11. Y. Li, R. Y. North, L. D. Rhines, C. E. Tatsui, G. Rao, D. D. Edwards, R. M. Cassidy, D. S. Harrison, C. A. Johansson, H. Zhang, P. M. Dougherty, DRG voltage-gated sodium channel 1.7 is upregulated in paclitaxel-induced neuropathy in rats and in humans with neuropathic pain. *Journal of Neuroscience* **38**, 1124–1136 (2018).

12. M. A. Odem, A. G. Bavencoffe, R. M. Cassidy, E. R. Lopez, J. Tian, C. W. Dessauer, E. T. Walters, Isolated nociceptors reveal multiple specializations for generating irregular ongoing activity associated with ongoing pain. *Pain* **159**, 2347–2362 (2018).

13. J. Yi, Z. Bertels, J. S. Del Rosario, A. J. Widman, R. A. Slivicki, M. Payne, H. M. Susser, B. A. Copits, R. W. Gereau, Bradykinin receptor expression and bradykinin-mediated sensitization of human sensory neurons. *Pain* **165**, 202 (2023).

14. D. Usoskin, A. Furlan, S. Islam, H. Abdo, P. Lönnerberg, D. Lou, J. Hjerling-Leffler, J. Haeggström, O. Kharchenko, P. V Kharchenko, S. Linnarsson, P. Ernfors, Unbiased classification of sensory neuron types by large-scale single-cell RNA sequencing. *Nat. Neurosci.* **18**, 145–153 (2015).

15. J. D. Silverman, L. Kruger, Selective neuronal glycoconjugate expression in sensory and autonomic ganglia: relation of lectin reactivity to peptide and enzyme markers. *J. Neurocytol.* **19**, 789–801 (1990).

16. S. N. Lawson, X. Fang, L. Djouhri, Nociceptor subtypes and their incidence in rat lumbar dorsal root ganglia (DRGs): focussing on C-polymodal nociceptors, Aβ-nociceptors, moderate pressure receptors and their receptive field depths. *Curr. Opin. Physiol.* **11**, 125–146 (2019).

17. X. Fang, L. Djouhri, S. McMullan, C. Berry, K. Okuse, S. G. Waxman, S. N. Lawson, trkA Is Expressed in Nociceptive Neurons and Influences Electrophysiological Properties via Nav1.8 Expression in Rapidly Conducting Nociceptors. *Journal of Neuroscience* **25**, 4868–4878 (2005).

18. X. Fang, L. Djouhri, S. McMullan, C. Berry, S. G. Waxman, K. Okuse, S. N. Lawson, Intense isolectin-B4 binding in rat dorsal root ganglion neurons distinguishes C-fiber nociceptors with broad action potentials and high Nav1.9 expression. *J. Neurosci.* **26**, 7281–7292 (2006).

19. S. Averill, S. B. McMahon, D. O. Clary, L. F. Reichardt, J. V. Priestley, Immunocytochemical Localization of trkA Receptors in Chemically Identified Subgroups of Adult Rat Sensory Neurons. *European Journal of Neuroscience* **7**, 1484–1494 (1995).

20. H. Wang, M. J. Zylka, Mrgprd-expressing polymodal nociceptive neurons innervate most known classes of substantia gelatinosa neurons. *Journal of Neuroscience* **29**, 13202–13209 (2009).

21. M. J. Zylka, F. L. Rice, D. J. Anderson, Topographically Distinct Epidermal Nociceptive Circuits Revealed by Axonal Tracers Targeted to Mrgprd. *Neuron* **45**, 17–25 (2005).

22. E. S. McCoy, B. Taylor-Blake, M. J. Zylka, CGRPα-expressing sensory neurons respond to stimuli that evoke sensations of pain and itch. *PLoS One* **7** (2012).

23. W. Luo, S. R. Wickramasinghe, J. M. Savitt, J. W. Griffin, T. M. Dawson, D. D. Ginty, A Hierarchical NGF Signaling Cascade Controls Ret-Dependent and Ret-Independent Events during Development of Nonpeptidergic DRG Neurons. *Neuron* **54**, 739–754 (2007).

24. B. Abrahamsen, J. Zhao, C. O. Asante, C. M. Cendan, S. Marsh, J. P. Martinez-Barbera, M. A. Nassar, A. H. Dickenson, J. N. Wood, The Cell and Molecular Basis of Mechanical, Cold, and Inflammatory Pain. *Science (1979).* **321**, 702–705 (2008).

25. Y. Zheng, P. Liu, L. Bai, J. S. Trimmer, B. P. Bean, D. D. Ginty, Deep Sequencing of Somatosensory Neurons Reveals Molecular Determinants of Intrinsic Physiological Properties. *Neuron* **103**, 598-616.e7 (2019).

26. M. J. Patil, A. H. Hovhannisyan, A. N. Akopian, Characteristics of sensory neuronal groups in CGRP-cre-ER reporter mice: Comparison to Nav1.8-cre, TRPV1-cre and TRPV1-GFP mouse lines. *PLoS One* **13** (2018).

27. D. Tavares-Ferreira, S. Shiers, P. R. Ray, A. Wangzhou, V. Jeevakumar, I. Sankaranarayanan, A. M. Cervantes, J. C. Reese, A. Chamessian, B. A. Copits, P. M. Dougherty, R. W. Gereau IV, M. D. Burton, G. Dussor, T. J. Price, Spatial transcriptomics of dorsal root ganglia identifies molecular signatures of human nociceptors. *Sci. Transl. Med.* **14**, 8186 (2022).

28. M. Jung, M. Dourado, J. Maksymetz, A. Jacobson, B. I. Laufer, M. Baca, O. Foreman, D. H. Hackos, L. Riol-Blanco, J. S. Kaminker, Cross-species transcriptomic atlas of dorsal root ganglia reveals species-specific programs for sensory function. *Nat. Commun.* **14**, 366 (2023).

29. M. Q. Nguyen, L. J. von Buchholtz, A. N. Reker, N. J. J. P. Ryba, S. Davidson, Single-nucleus transcriptomic analysis of human dorsal root ganglion neurons. *Elife* **10**, 1–21 (2021).

30. S. A. Bhuiyan, M. Xu, L. Yang, E. Semizoglou, P. Bhatia, J. M. Mwirigi, I. Sankaranarayanan, D. Tavares-ferreira, U. Green, R. A. Slivicki, J. Yi, C. J. Woolf, J. K. Lennerz, J. L. Whited, Harmonized cross-species cell atlases of trigeminal and dorsal root ganglia. *bioRxiv*, doi: https://doi.org/10.1101/2023.07.04.547740 (2023).

31. S. Shiers, R. M. Klein, T. J. Price, Quantitative differences in neuronal subpopulations between mouse and human dorsal root ganglia demonstrated with RNAscope in situ hybridization. *Pain* **161**, 2410–2424 (2020).

32. M. Q. Nguyen, L. J. von Buchholtz, A. N. Reker, N. J. J. P. Ryba, S. Davidson, Single-nucleus transcriptomic analysis of human dorsal root ganglion neurons. *Elife* **10**, 1–21 (2021).

33. H. Yu, S. S. Nagi, D. Usoskin, Y. Hu, J. Kupari, O. Bouchatta, H. Yan, S. L. Cranfill, M. Gautam, Y. Su, Y. Lu, J. Wymer, M. Glanz, P. Albrecht, H. Song, G. L. Ming, S. Prouty, J. Seykora, H. Wu, M. Ma, A. Marshall, F. L. Rice, M. Li, H. Olausson, P. Ernfors, W. Luo, Leveraging deep single-soma RNA sequencing to explore the neural basis of human somatosensation. *Nature Neuroscience 2024 27:12* **27**, 2326–2340 (2024).

34. D. Tavares-Ferreira, S. Shiers, P. R. Ray, A. Wangzhou, V. Jeevakumar, I. Sankaranarayanan, A. M. Cervantes, J. C. Reese, A. Chamessian, B. A. Copits, P. M. Dougherty, R. W. Gereau IV, M. D. Burton, G. Dussor, T. J. Price, Spatial transcriptomics of dorsal root ganglia identifies molecular signatures of human nociceptors. *Sci. Transl. Med.* **14**, 8186 (2022).

35. C. Rostock, K. Schrenk-Siemens, J. Pohle, J. Siemens, Human vs. Mouse Nociceptors – Similarities and Differences. *Neuroscience* **387**, 13–27 (2018).

36. S. A. Bhuiyan, M. Xu, L. Yang, E. Semizoglou, P. Bhatia, K. I. Pantaleo, I. Tochitsky, A. Jain, B. Erdogan, S. Blair, V. Cat, J. M. Mwirigi, I. Sankaranarayanan, D. Tavares-Ferreira, U. Green, L. A. McIlvried, B. A. Copits, Z. Bertels, J. S. Del Rosario, A. J. Widman, R. A. Slivicki, J. Yi, R. Sharif-Naeini, C. J. Woolf, J. K. Lennerz, J. L. Whited, T.

946 J. Price, R. W. Gereau, W. Renthal, Harmonized cross-species cell atlases of trigeminal
947 and dorsal root ganglia. *Sci. Adv.* **10** (2024).

948 37. S. A. Bhuiyan, S. S. Nagi, I. Sankaranarayanan, E. Semizoglou, D. Usoskin, L. Yang, H.
949 Yu, A. Arendt-Tranholm, Z. Bertels, P. Bhatia, O. Bouchatta, K. Boyer, A. Cervantes, J.
950 Chalif, H. Chintalapudi, A. Cicalo, B. Copits, C. Cronin, M. Curatolo, X. Dong, P. M.
951 Dougherty, A. Dourson, G. Funk, K. Gabriel, D. S. Griesemer, H. Guo, P. Gupta, C.
952 Hofstetter, P. Horton, A. Hsieh, N. N. Inturi, A. Jain, S. Jayakar, B. Johnston, R. Kim, D.
953 Krauter, J. Kupari, J. Lemen, J. B. Lesnak, W. Liu, I. Lopez, Y. Lu, H. J. MacMillan, K.
954 Mazhar, P. Meriau, J. R. Moffitt, M. M. Moreno, J. M. Mwirigi, H. Naz, J. O'Brein, M.
955 Payne, J. Del Rosario, S. F. Rosen, S. Shiers, E. Simpson, R. Slivicki, J. R. Stone, D.
956 Tavares-Ferreira, M. Uhelski, C. J. Woolf, Q. Xu, J. Yi, M. S. Yousuf, D. Zhu, V. Cavalli, G.
957 Zhao, H. Olausson, P. Ernfors, I. Robert W Gereau, W. Luo, T. J. Price, W. Renthal, N. P.
958 H. P. Network, A Reference Atlas of the Human Dorsal Root Ganglion. *bioRxiv*, doi:
959 10.1101/2025.11.05.686654 (2025).

960 38. S. Davidson, B. A. Copits, J. Zhang, G. Page, A. Ghetti, R. W. Gereau, Human sensory
961 neurons: Membrane properties and sensitization by inflammatory mediators. *Pain* **155**,
962 1861–1870 (2014).

963 39. C. R. Cadwell, A. Palasantza, X. Jiang, P. Berens, Q. Deng, M. Yilmaz, J. Reimer, S.
964 Shen, M. Bethge, K. F. Tolias, R. Sandberg, A. S. Tolias, Electrophysiological,
965 transcriptomic and morphologic profiling of single neurons using Patch-seq. *Nat.*
966 *Biotechnol.* **34**, 199–203 (2016).

967 40. T. Parpaite, L. Brosse, N. Séjourné, A. Laur, Y. Mechioukhi, P. Delmas, B. Coste, Patch-
968 seq of mouse DRG neurons reveals candidate genes for specific mechanosensory
969 functions. *Cell Rep.* **37** (2021).

970 41. H. Yu, D. Usoskin, S. S. Nagi, Y. Hu, J. Kupari, O. Bouchatta, S. L. Cranfill, Y. Su, Y. Lv,
971 H. Song, G. Ming, S. Prouty, J. Seykora, H. Wu, M. Ma, H. Olausson, P. Ernfors, W. Luo,
972 Single-Soma Deep RNA sequencing of Human DRG Neurons Reveals Novel Molecular
973 and Cellular Mechanisms Underlying Somatosensation. *bioRxiv*, doi:
974 doi.org/10.1101/2023.03.17.533207 (2023).

975 42. O. Avraham, A. Chamessian, R. Feng, L. Yang, A. E. Halevi, A. M. Moore, R. W. Gereau,
976 V. Cavalli, Profiling the molecular signature of satellite glial cells at the single cell level
977 reveals high similarities between rodents and humans. *Pain* **163**, 2348–2364 (2022).

978 43. W. Renthal, I. Tochitsky, L. Yang, Y. C. Cheng, E. Li, R. Kawaguchi, D. H. Geschwind, C.
979 J. Woolf, Transcriptional reprogramming of distinct peripheral sensory neuron subtypes
980 after axonal injury. *Neuron* **108**, 128 (2020).

981 44. N. Sharma, K. Flaherty, K. Lezgiyeva, D. E. Wagner, A. M. Klein, D. D. Ginty, The
982 emergence of transcriptional identity in somatosensory neurons. *Nature* **577**, 392–398
983 (2020).

984 45. L. Djouhri, S. N. Lawson, Aβ-fiber nociceptive primary afferent neurons: A review of
985 incidence and properties in relation to other afferent A-fiber neurons in mammals. *Brain*
986 *Res. Rev.* **46**, 131–145 (2004).

46. L. Yang, M. Xu, S. A. Bhuiyan, J. Li, J. Zhao, R. J. Cohrs, J. T. Susterich, S. Signorelli, U. Green, J. R. Stone, D. Levy, J. K. Lennerz, W. Renthal, Human and mouse trigeminal ganglia cell atlas implicates multiple cell types in migraine. *Neuron*, 1–16 (2022).

47. D. Hoy, L. March, P. Brooks, F. Blyth, A. Woolf, C. Bain, G. Williams, E. Smith, T. Vos, J. Barendregt, C. Murray, R. Burstein, R. Buchbinder, The global burden of low back pain: Estimates from the Global Burden of Disease 2010 study. *Ann. Rheum. Dis.* **73**, 968–974 (2014).

48. J. W. Lucas, I. Sohi, Chronic Pain and High-impact Chronic Pain Among U.S. Adults, 2023. National Center for Health Statistics [Preprint] (2024). https://doi.org/10.15620/CDC/169630.

49. D. L. Bennett, X. A. J. Clark, J. Huang, S. G. Waxman, S. D. Dib-Hajj, The role of voltage-gated sodium channels in pain signaling. *Physiol. Rev.* **99**, 1079–1151 (2019).

50. D. T. Jones, N. A. Zurek, S. R. A. Alles, Shaping the Action Potential in Dorsal Root and Trigeminal Ganglia Neurons: Relevance to Pain Mechanisms. *J. Neurosci.* **46**, e0926252025 (2026).

51. Y. Li, R. Y. North, L. D. Rhines, C. E. Tatsui, G. Rao, D. D. Edwards, R. M. Cassidy, D. S. Harrison, C. A. Johansson, H. Zhang, P. M. Dougherty, DRG voltage-gated sodium channel 1.7 is upregulated in paclitaxel-induced neuropathy in rats and in humans with neuropathic pain. *Journal of Neuroscience* **38**, 1124–1136 (2018).

52. L. Djouhri, R. Newton, S. R. Levinson, C. M. Berry, B. Carruthers, S. N. Lawson, Sensory and electrophysiological properties of guinea-pig sensory neurones expressing Nav 1.7 (PN1) Na+ channel α subunit protein. *Journal of Physiology* **546**, 565–576 (2003).

53. S. D. Dib-Hajj, L. Tyrrell, T. R. Cummins, J. A. Black, P. M. Wood, S. G. Waxman, Two tetrodotoxin-resistant sodium channels in human dorsal root ganglion neurons. *FEBS Lett.* **462**, 117–120 (1999).

54. S. C. Benn, M. Costigan, S. Tate, M. Fitzgerald, C. J. Woolf, Developmental Expression of the TTX-Resistant Voltage-Gated Sodium Channels Na v 1.8 (SNS) and Na v 1.9 (SNS2) in Primary Sensory Neurons. *The Journal of Neuroscience* **21**, 6077–6085 (2001).

55. S. D. Dib-Hajj, L. Tyrrell, J. A. Black, S. G. Waxman, NaN, a novel voltage-gated Na channel, is expressed preferentially in peripheral sensory neurons and down-regulated after axotomy. *Proc. Natl. Acad. Sci. U. S. A.* **95**, 8963–8968 (1998).

56. J. Fjell, P. Hjelmström, W. Hormuzdiar, M. Milenkovic, F. Aglieco, L. Tyrrell, S. Dib-Hajj, S. G. Waxman, J. A. Black, Localization of the tetrodotoxin-resistant sodium channel NaN in nociceptors. *Neuroreport* **11**, 199–202 (2000).

57. Y. Zheng, P. Liu, L. Bai, J. S. Trimmer, B. P. Bean, D. D. Ginty, Deep Sequencing of Somatosensory Neurons Reveals Molecular Determinants of Intrinsic Physiological Properties. *Neuron* **103**, 598-616.e7 (2019).

58. P. Ray, A. Torck, L. Quigley, A. Wangzhou, M. Neiman, C. Rao, T. Lam, J. Y. Kim, T. H. Kim, M. Q. Zhang, G. Dussor, T. J. Price, Comparative transcriptome profiling of the

1027 human and mouse dorsal root ganglia: An RNA-seq-based resource for pain and sensory
1028 neuroscience research. *Pain* **159**, 1325–1345 (2018).

1029 59. M. J. Craner, J. P. Klein, M. Renganathan, J. A. Black, S. G. Waxman, Changes of
1030 sodium channel expression in experimental painful diabetic neuropathy. *Ann. Neurol.* **52**,
1031 786–792 (2002).

1032 60. L. A. McIlvried, J. S. Del Rosario, M. Y. Pullen, A. Wangzhou, T. D. Sheahan, A. J.
1033 Shepherd, R. A. Slivicki, J. A. Lemen, T. J. Price, B. A. Copits, R. W. Gereau, Intrinsic
1034 adaptive plasticity in mouse and human sensory neurons. *J. Gen. Physiol.* **157**,
1035 e202313488 (2024).

1036 61. N. A. Zurek, R. Ehsanian, A. E. Goins, I. M. Adams, T. Petersen, S. Goyal, M. Shilling, K.
1037 N. Westlund, S. R. A. Alles, Electrophysiological Analyses of Human Dorsal Root Ganglia
1038 and Human Induced Pluripotent Stem Cell-derived Sensory Neurons From Male and
1039 Female Donors. *Journal of Pain*, doi: 10.1016/j.jpain.2023.12.008 (2023).

1040 62. A. Bavencoffe, E. A. Spence, M. Y. Zhu, A. Garza-Carbajal, K. E. Chu, O. E. Bloom, C. W.
1041 Dessauer, E. T. Walters, Macrophage Migration Inhibitory Factor (MIF) Makes Complex
1042 Contributions to Pain-Related Hyperactivity of Nociceptors after Spinal Cord Injury.
1043 *Journal of Neuroscience* **42**, 5463–5480 (2022).

1044 63. W. Renthal, I. Tochitsky, L. Yang, Y.-C. Cheng, E. Li, R. Kawaguchi, D. H. Geschwind, C.
1045 J. Woolf, Transcriptional Reprogramming of Distinct Peripheral Sensory Neuron Subtypes
1046 after Axonal Injury. *Neuron* **108**, 128–144 (2020).

1047 64. V. Truong, J. Brougher, T. Strassmaier, I. Lu, D. George, T. J. Price, A. Obergrussberger,
1048 A. Randolph, R. J. Haedo, N. Fertig, P. Walsh, Transcriptomic analysis and high
1049 throughput functional characterization of human induced pluripotent stem cell derived
1050 sensory neurons. *bioRxiv*, 2024.08.23.607310 (2024).

1051 65. T. P. Harty, S. G. Waxman, Inactivation properties of sodium channel Nav1.8 maintain
1052 action potential amplitude in small DRG neurons in the context of depolarization. *Mol.*
1053 *Pain* **3**, 12 (2007).

1054 66. X. Weng, T. Smith, J. Sathish, L. Djouhri, Chronic inflammatory pain is associated with
1055 increased excitability and hyperpolarization-activated current (Ih) in C- but not Aδ-
1056 nociceptors. *Pain* **153**, 900–914 (2012).

1057 67. L. Djouhri, M. Al Otaibi, K. Kahlat, T. Smith, J. Sathish, X. Weng, Persistent hindlimb
1058 inflammation induces changes in activation properties of hyperpolarization-activated
1059 current (Ih) in rat C-fiber nociceptors in vivo. *Neuroscience* **301**, 121–133 (2015).

1060 68. H. Zhang, T. Kashihara, T. Nakada, S. Tanaka, K. Ishida, S. Fuseya, H. Kawagishi, K.
1061 Kiyosawa, M. Kawamata, M. Yamada, Prostanoid EP4 receptor-mediated augmentation
1062 of IH currents in Ab dorsal root ganglion neurons underlies neuropathic pains. *Journal of*
1063 *Pharmacology and Experimental Therapeutics* **368**, 50–58 (2019).

1064 69. C. E. Payne, A. R. Brown, J. W. Theile, A. J. C. Loucif, A. J. Alexandrou, M. D. Fuller, J.
1065 H. Mahoney, B. M. Antonio, A. C. Gerlach, D. M. Printzenhoff, R. L. Prime, G.
1066 Stockbridge, A. J. Kirkup, A. W. Bannon, S. England, M. L. Chapman, S. Bagal, R.
1067 Roeloffs, U. Anand, P. Anand, P. J. Bungay, M. Kemp, R. P. Butt, E. B. Stevens, A novel

1068 selective and orally bioavailable Nav1.8 channel blocker, PF-01247324, attenuates
1069 nociception and sensory neuron excitability. *Br. J. Pharmacol.* **172**, 2654–2670 (2015).

1070 70. X. F. Zhang, C. C. Shieh, M. L. Chapman, M. A. Matulenko, A. H. Hakeem, R. N.
1071 Atkinson, M. E. Kort, B. E. Marron, S. Joshi, P. Honore, C. R. Faltynek, D. S. Krafte, M. F.
1072 Jarvis, A-887826 is a structurally novel, potent and voltage-dependent Nav1.8 sodium
1073 channel blocker that attenuates neuropathic tactile allodynia in rats. *Neuropharmacology*
1074 **59**, 201–207 (2010).

1075 71. M. E. Kort, R. N. Atkinson, J. B. Thomas, I. Drizin, M. S. Johnson, M. A. Secrest, R. J.
1076 Gregg, M. J. C. Scanio, L. Shi, A. H. Hakeem, M. A. Matulenko, M. L. Chapman, M. J.
1077 Krambis, D. Liu, C. C. Shieh, X. Zhang, G. Simler, J. P. Mikusa, C. Zhong, S. Joshi, P.
1078 Honore, R. Roeloffs, S. Werness, B. Antonio, K. C. Marsh, C. R. Faltynek, D. S. Krafte,
1079 M. F. Jarvis, B. E. Marron, Subtype-selective Nav1.8 sodium channel blockers:
1080 Identification of potent, orally active nicotinamide derivatives. *Bioorg. Med. Chem. Lett.*
1081 **20**, 6812–6815 (2010).

1082 72. M. S. Gold, D. Weinreich, C. S. Kim, R. Wang, J. Treanor, F. Porreca, J. Lai,
1083 Redistribution of Nav1.8 in uninjured axons enables neuropathic pain. *Journal of*
1084 *Neuroscience* **23**, 158–166 (2003).

1085 73. C. G. Faber, J. G. J. Hoeijmakers, H. S. Ahn, X. Cheng, C. Han, J. S. Choi, M. Estacion,
1086 G. Lauria, E. K. Vanhoutte, M. M. Gerrits, S. Dib-Hajj, J. P. H. Drenth, S. G. Waxman, I. S.
1087 J. Merkies, Gain of function Na V1.7 mutations in idiopathic small fiber neuropathy. *Ann.*
1088 *Neurol.* **71**, 26–39 (2012).

1089 74. Y. Yang, J. Huang, M. A. Mis, M. Estacion, L. Macala, P. Shah, B. R. Schulman, D. B.
1090 Horton, S. D. Dib-Hajj, S. G. Waxman, Nav1.7-A1632G Mutation from a Family with
1091 Inherited Erythromelalgia: Enhanced Firing of Dorsal Root Ganglia Neurons Evoked by
1092 Thermal Stimuli. *The Journal of Neuroscience* **36**, 7511 (2016).

1093 75. M. R. Ghovanloo, P. R. Effraim, J. H. Yuan, B. R. Schulman, D. S. Jacobs, S. D. Dib-Hajj,
1094 S. G. Waxman, Nav1.7 P610T mutation in two siblings with persistent ocular pain after
1095 corneal axon transection: impaired slow inactivation and hyperexcitable trigeminal
1096 neurons. *J. Neurophysiol.* **129**, 609–618 (2023).

1097 76. C. G. Faber, G. Lauria, I. S. J. Merkies, X. Cheng, C. Han, H. S. Ahn, A. K. Persson, J. G.
1098 J. Hoeijmakers, M. M. Gerrits, T. Pierro, R. Lombardi, D. Kapetis, S. D. Dib-Hajj, S. G.
1099 Waxman, Gain-of-function Nav1.8 mutations in painful neuropathy. *Proc. Natl. Acad. Sci.*
1100 *U. S. A.* **109**, 19444–19449 (2012).

1101 77. Vertex Announces Positive Results From the VX-548 Phase 3 Program for the Treatment
1102 of Moderate-to-Severe Acute Pain | Vertex Pharmaceuticals, *Vertex Press Release*
1103 (2024). https://investors.vrtx.com/news-releases/news-release-details/vertex-announces-
1104 positive-results-vx-548-phase-3-program.

1105 78. J. Jones, D. J. Correll, S. M. Lechner, I. Jazic, X. Miao, D. Shaw, C. Simard, J. D. Osteen,
1106 B. Hare, A. Beaton, T. Bertoch, A. Buvanendran, A. S. Habib, L. J. Pizzi, R. A. Pollak, S.
1107 G. Weiner, C. Bozic, P. Negulescu, P. F. White, Selective Inhibition of Na V 1.8 with VX-
1108 548 for Acute Pain . *New England Journal of Medicine* **389**, 393–405 (2023).

79. M. V. Valtcheva, B. A. Copits, S. Davidson, T. D. Sheahan, M. Y. Pullen, J. G. McCall, K. Dikranian, R. W. Gereau, Surgical extraction of human dorsal root ganglia from organ donors and preparation of primary sensory neuron cultures. *Nat. Protoc.* **11**, 1877–1888 (2016).

80. Y. Hao, S. Hao, E. Andersen-Nissen, W. M. Mauck, S. Zheng, A. Butler, M. J. Lee, A. J. Wilk, C. Darby, M. Zager, P. Hoffman, M. Stoeckius, E. Papalexi, E. P. Mimitou, J. Jain, A. Srivastava, T. Stuart, L. M. Fleming, B. Yeung, A. J. Rogers, J. M. McElrath, C. A. Blish, R. Gottardo, P. Smibert, R. Satija, Integrated analysis of multimodal single-cell data. *Cell* **184**, 3573 (2021).

1120 **Table 1. Summary of hDRG donor demographic information**

N	56
Race	
White	42
Black	12
Other/Unknown	2
Sex	
Male	35
Female	21
Cause of Death	
Anoxia	25
Stroke	19
Head Trauma	11
Other/Unknown	1
Age (years) †	45.63±15.28
Body mass index †	28.22±6.87

1121 †Displayed in Mean ± SD

1122 **Table 1. Summary of electrophysiological characteristics of each E-type**

	E-type 1 (n=33)	E-type 2 (n=74)	E-type 3 (n=121)
Resting membrane potential (mV)*	-48.56 ± 1.59	-51.72 ± 1.50	-54.59 ± 0.57
Input resistance (MΩ)*	94.48 ± 10.96	158.6 ± 12.87	68.00 ± 5.49
Voltage sag ratio**	0.24 ± 0.03	0.33 ± 0.02	0.45 ± 0.01
Rheobase (pA)**	1359.84 ± 104.35	322.95 ± 27.01	1037.02 ± 61.28
AP threshold (mV)**	-7.85 ± 2.01	-16.77 ± 0.91	-21.84 ± 0.91
AP Amplitude (mV)**	29.49 ± 2.27	68.13 ± 1.14	72.23 ± 1.02
AP Peak (overshoot; mV)**	22.28 ± 2.65	51.36 ± 0.97	50.68± 0.86
Half-width (ms)**	2.72 ± 0.25	5.25 ± 0.27	2.23 ± 0.09
Rise time (ms)**	1.21 ± 0.14	0.81 ± 0.03	0.68 ± 0.06
Decay time (ms)**	4.33 ± 0.43	9.74 ± 0.46	3.87 ± 0.17

1123 *$p<0.001$, **$p<0.0001$; ANOVA or Kruskall-Wallis test

1124 **Table 3. Description of pain history in Pain Hx donors**

Pain history description	Number of cells patched	Included in RNAScope
Constant joint pain since age 17	0	x
Leg pain and scleroderma, prescribed pain medication	2	
History of multiple back surgeries, arthritis, bulging disc, back injury. Used prescribed pain medication for >5 years.	3	
Knee pain due to arthritis	1	
Knee pain due to tendonitis from playing football	1	
Severe pain in the groin causing difficulty walking. Occasional migraines and pain in back of the neck.	1	
Arthritis; history of knee surgery and prospective hip replacement surgery.	2	x
Degenerative disk disease; nerve block injections for back pain.	8	x
Arthritis; prescribed pain medication	1	
knee pain, finger joint pain (unspecified laterality). "R hip problem" with neuropathy	2	
Bulging lumbar disc managed with steroid injections in back and acetaminophen-hydrocodone	1	
Fibromyalgia, osteoarthritis, rheumatoid/psoriatic arthritis with hx of R and L knee arthroscopy. Home medications include gabapentin, oxycodone HCL	0	
Lower back pain managed by pain clinic, home medication includes Percocet	16	

1125

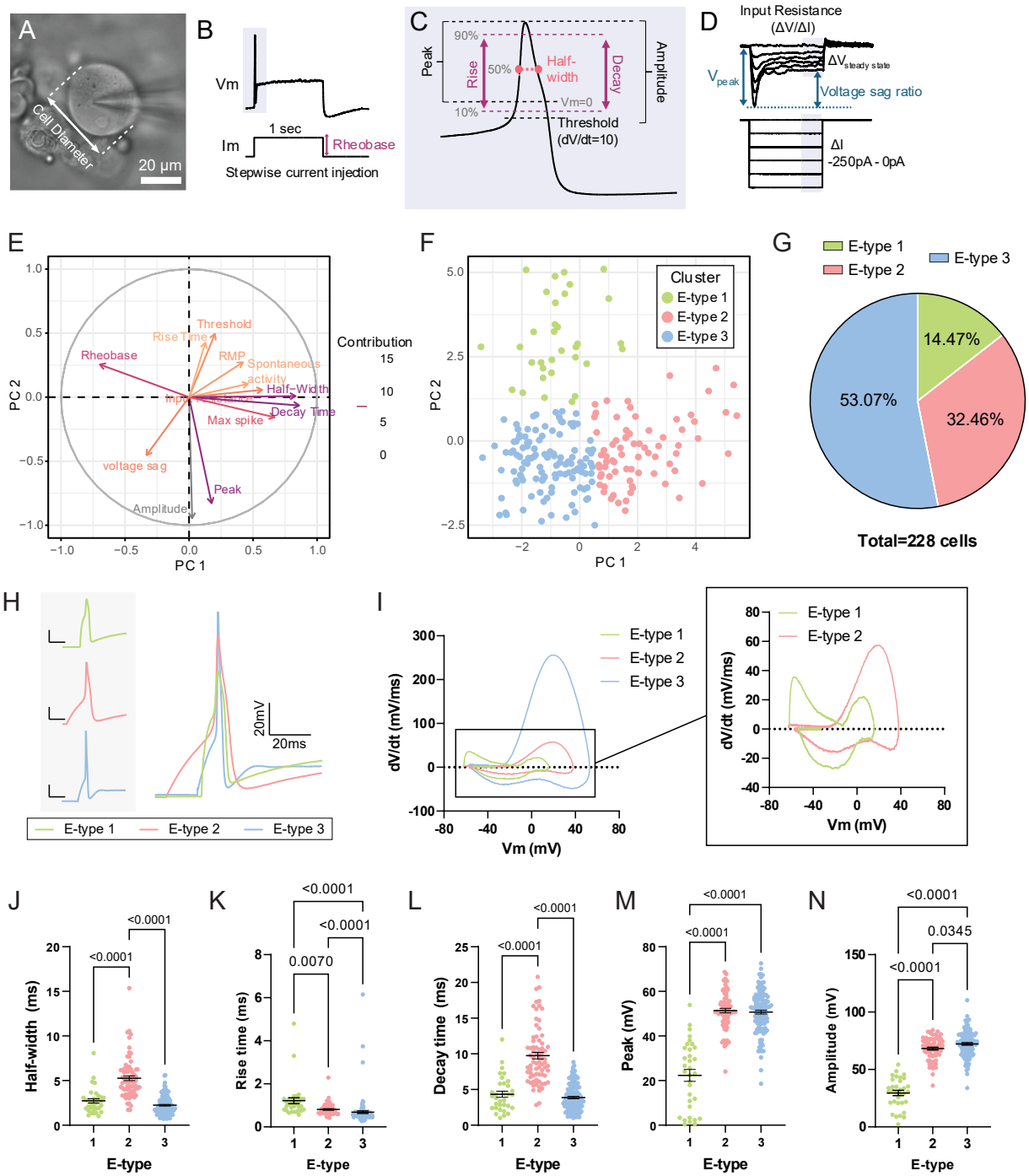

Fig. 1. Human DRG exhibit three electrophysiologically defined cell types (E-types).
(**A**) Image of cultured hDRG neuron recorded for this study.
(**B**) Example action potential (AP) voltage trace (Vm, top) in response to a 1-second depolarizing current injection (Im, bottom) at threshold (rheobase).
(**C**) Example AP trace illustrating waveform properties used for analysis.
(**D**) Example voltage traces in response to hyperpolarizing current injections illustrating the quantification of input resistance and voltage sag ratio.

(**E**) Principal component analysis (PCA) loading plot of demonstrating the relative contribution of each electrical property to each principal component. Membrane properties and spike kinetic parameters were used as variables for PCA. RMP, resting membrane potential.
(**F**) Score plot of individual hDRG neurons, which clustered into three groups (E-types) based on their electrical properties. Each sample is colored by its E-type.
(**G**) Pie chart depicting the percentage of hDRG neurons in each E-type cluster from a total of 228 recordings obtained from 56 independent donros.
(**H**) Representative traces of AP waveforms from each E-type, shown in separate (left) and in overlay (right).
(**I**) Representative phase-plane plots of the AP waveforms for each E-type.
(**J-N**) Summary graphs of AP properties across the three E-types. N=33 (E-type 1), 74 (E-type 2), and 121 neurons (E-type 3). Bonferroni correction for multiple comparisons were used to determine threshold for statistical significance ($\alpha=0.005$) for group comparisons using Kruskall-Wallis or ANOVA tests. P-values for Dunn's post-hoc test are shown in plot.
(**J**) AP half-width, $p<0.0001$ (significant), Kruskall-Wallis test.
(**K**) Rise-time, $p<0.0001$ (significant), Kruskall-Wallis test.
(**L**) AP decay time, $p<0.0001$ (significant), Kruskall-Wallis test.
(**M**) Peak overshoot, $p<0.0001$ (significant), Kruskall-Wallis test.
(**N**) AP rise-time, $p<0.0001$ (significant), Kruskall-Wallis test.

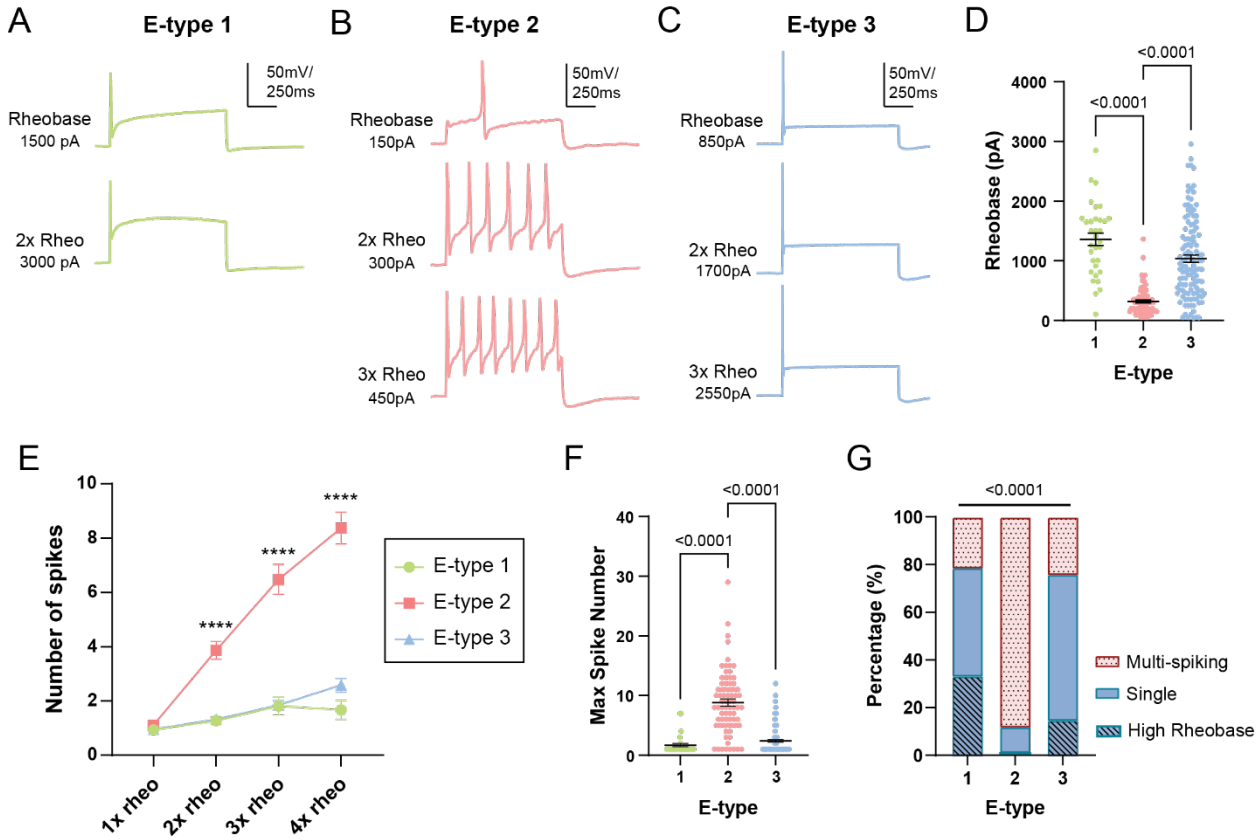

Fig. 2. Action potential firing patterns in hDRG E-types.
(**A-C**) Representative voltage traces of the AP waveforms in response to 1 second depolarizing current injections at threshold (rheobase) and suprathreshold (2-3x rheo) levels for each E-type.
(**D**) Summary graph of rheobase values for each E-type. p<0.0001 (significant), Kruskall-Wallis test. P-values for Dunn's post-hoc test are shown in plot.
(**E**) Input-output curves of the number of AP spikes in response to 1 second current injections of 1-4x rheobase for each E-type). Linear mixed-effects analysis revealed significant fixed effect (p<0.0001; significant) of current injection, E-type, and current injection x E-type interaction. ****p<0.0001 (significant), Tukey's multiple comparison test, E-type 1 vs. E-type 2, E-type 1 vs. E-type 3.
(**F**) Summary graph of the maximum AP spike number in response to supratheshold depolarizing current injections for each E-type. p<0.0001 (significant), Kruskall-Wallis test. P-values for Dunn's post-hoc test are shown in plot.
(**G**) Percentage of the AP firing patterns (multi-spiking, single, or high rheobase) across each E-type. P<0.0001, Chi-square test. N=33 (E-type 1), 74 (E-type 2), and 121 neurons (E-type 3). Sample sizes are N=33 (E-type 1), 74 (E-type 2), and 121 neurons (E-type 3; **D-G**) Bonferroni correction for multiple comparisons were used to determine threshold for statistical significance (α=0.005) for statistical comparisons reported in (**D-F**).

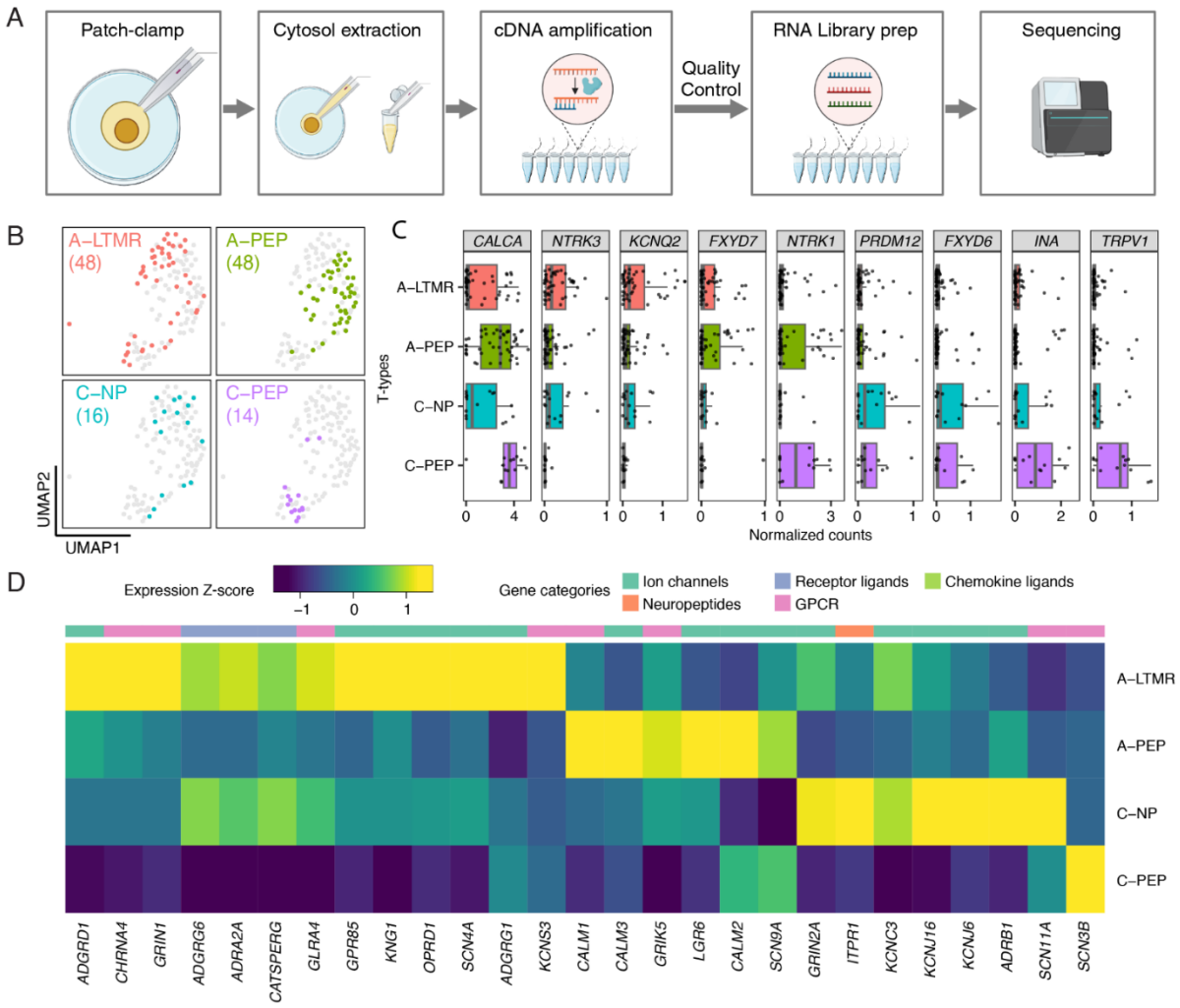

Fig. 3. Patch-seq recordings identify four hDRG neuronal T-types.
(**A**) Patch-seq workflow in human DRG neurons.
(**B**) Uniform Manifold Approximation and Projection (UMAP) plot of 126 human DRG Patch-seq samples assigned to neuronal clusters. Samples are colored by T-types by anchoring and label transfer from the hDRG single-soma RNA-seq data, and the numbers in the parentheses indicate cell counts in each cluster.
(**C**). Normalized counts (log2 transformed counts per million[log2CPM]) of select hDRG cell class marker genes in each T-type. Scatter plot indicates the expression in individual samples and the boxes indicate quartiles and whiskers are 1.5-times the interquartile range (Q1-Q3). The median is a grey line inside each box.
(**D**) Heatmap showing the scaled expression (Z-score of log2CPM) of DEGs across T-types.

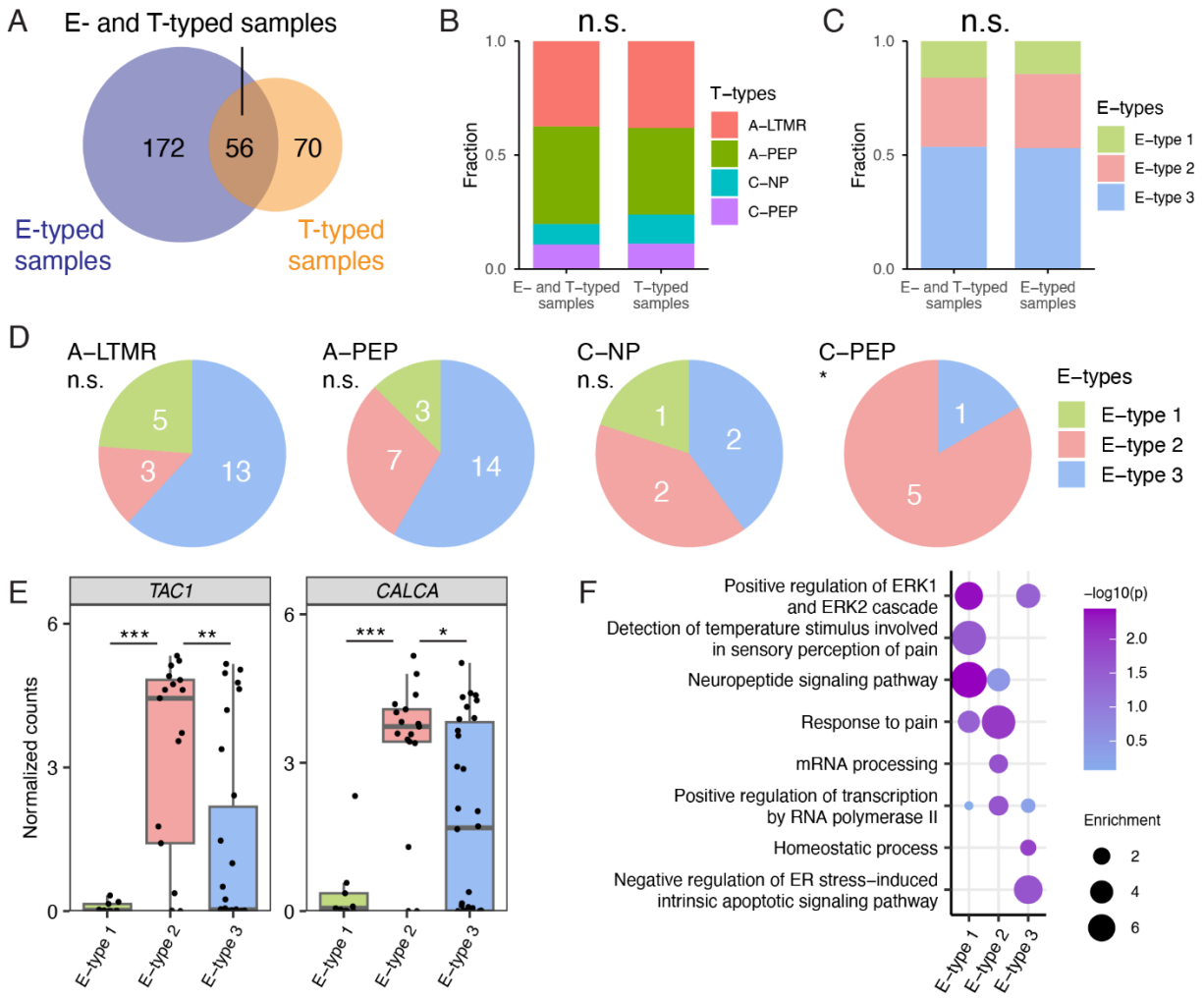

Fig. 4. Patch-seq links hDRG E-types to T-types.
(**A**) Venn diagram showing samples with E-types alone (included only in the electrophysiological analysis), samples with T-types alone (included only in the transcriptional analysis), and samples assigned both an E-type and T-type (included in both electrophysiological and transcriptional analyses).
(**B**) Bar plot of the T-type distribution between samples assigned with T-types only and samples with both E- and T-types. Chi-square test, p = 0.8076.
(**C**) Bar plot of E-type distribution between samples assigned with E-types only and samples with both E- and T-types. Chi-square test, p = 0.9129.
(**D**) Pie chart showing the distribution of E-types in each T-type. Chi-square tests, p = 0.2415 for A-LTMR, p = 0.8593 for A-PEP, p = 0.8195 for C-NP, and p = 0.018 (*) for C-PEP.
(**E**) Box plots showing the Normalized counts (log2 transformed counts per million[log2CPM]) of *TAC1* and *CALCA* across E-types. Scatter plots indicate the expression in individual samples and the boxes indicate quartiles and whiskers are 1.5-times the interquartile range (Q1-Q3). The median is a grey line inside each box. One-way ANOVA, p = 0.000212 for *TAC1* (***), and p = 0.000165 for *CALCA* (***).
(**F**) Enriched gene ontology terms (p<0.05, enrichment > 1.5) across E-types.

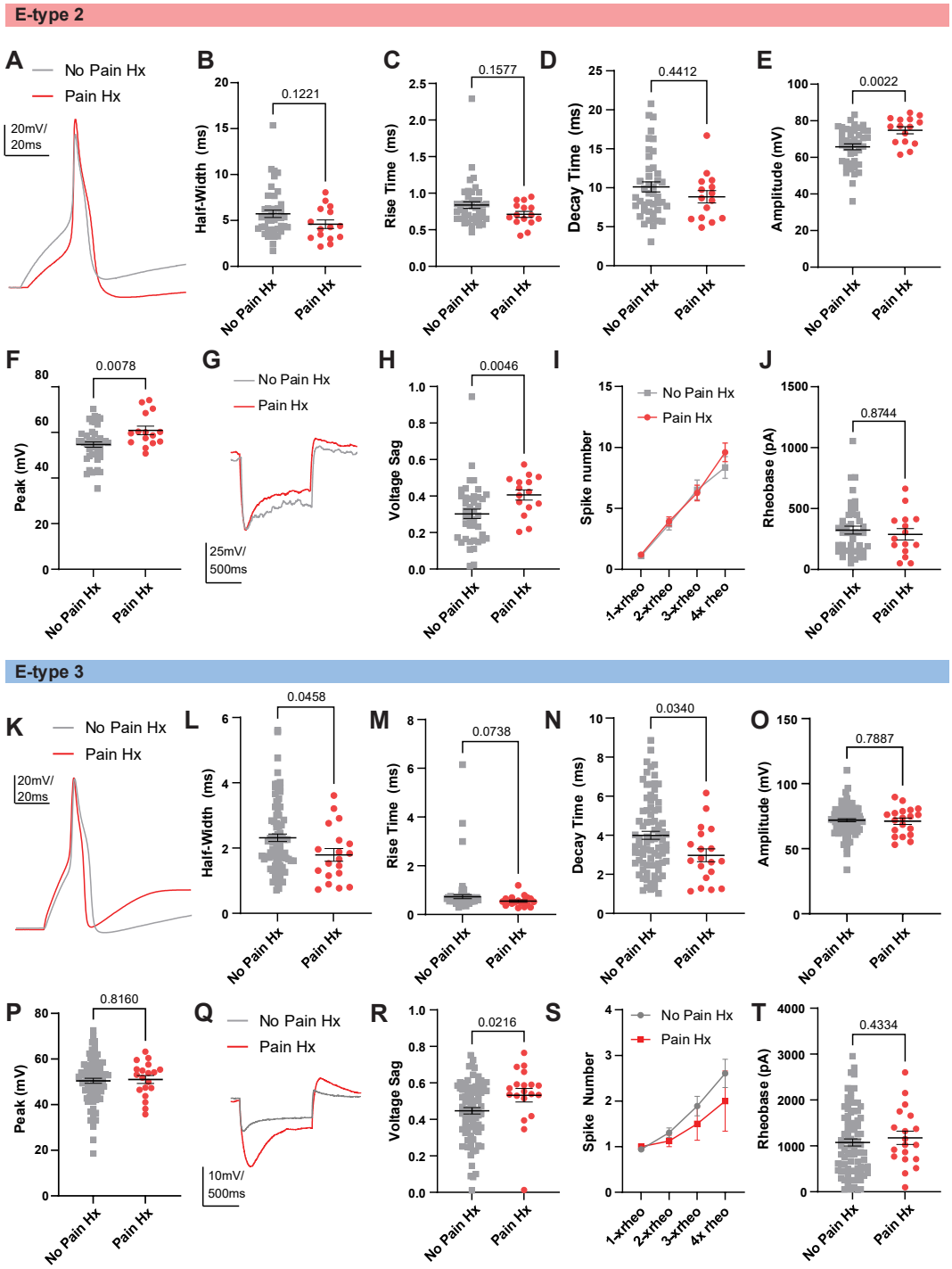

Fig. 5. hDRG from donors with prior pain history exhibit E-type specific differences in their electrical properties.

(**A-J**) Intrinsic membrane properties and AP kinetics of E-type 2 hDRG neurons, separated by donor history. N=42 (No Pain Hx), 15 (Pain hx). Bonferroni correction for multiple comparisons were used to determine the threshold for statistical significance (α=0.005) for group comparisons.

(**A**) Representative AP traces elicited by 1 second depolarizing current injections at rheobase in hDRG E-type 2 neurons from donors with (red) and without (grey) prior pain history.

(**B-F**) Summary graphs of AP kinetics of E-type 2 hDRG neurons, separated by donor pain history.
(**B**) AP half-width; p=0.1221 (not significant), Mann-Whitney test.
(**C**) AP rise time; p=0.1557 (not significant), Mann-Whitney test.
(**D**) AP decay time; p=0.4412 (not significant), Mann-Whitney test.
(**E**) AP voltage amplitude from threshold; p=0.0022 (significant), Mann-Whitney test.
(**F**) AP Peak (overshoot); p=0.0078 (not significant), unpaired t-test.
(**G**) Example voltage traces of E-type 2 neurons in response to hyperpolarzing current injections in hDRG from donors with (red) and without (grey) prior pain history.
(**H-J**) Summary graphs showing voltage sag (H), input-output curves (I), and rheobase (J).
(**H**) Voltage sag in response to hyperpolarizing current injections; p=0.0046 (significant), Mann-Whitney test.
(**I**) Input-output curve showing number of spikes fired plotted against suprathreshold current injected. Mixed effects model analysis shows significant fixed effect of current injection ($p<0.0001$); fixed effects of pain history (p=0.5410) and the interaction of pain history x current injected (p=0.7277) were not significant.
(**J**) Rheobase; p=0.4334 (not significant), Mann-Whitney test.
(**K-T**) Intrinsic membrane properties and AP kinetics of E-type 3 hDRG neurons, separated by donor history. N=84 (No Pain Hx), 19 (Pain hx). Bonferroni correction for multiple comparisons were used to determine the threshold for statistical significance ($\alpha=0.005$) for group comparisons.
(**K**) Representative AP traces elicited by 1 second depolarizing current injections at rheobase in hDRG E-type 3 neurons from donors with (red) and without (grey) prior pain history.
(**L-P**) Summary graphs of AP kinetics of E-type 3 hDRG neurons, separated by donor pain history.
(**L**) AP half-width; p=0.0458 (not significant), Mann-Whitney test.
(**M**) AP rise time; p=0.0738 (not significant), Mann-Whitney test.
(**N**) AP decay time; p=0.0340 (not significant), Mann-Whitney test.
(**O**) AP voltage amplitude from threshold; p=0.7887 (not significant), unpaired t-test.
(**P**) AP Peak (overshoot); p=0.8160 (not significant), unpaired t-test.
(**Q**) Example voltage traces of E-type 3 neurons in response to hyperpolarzing current injections in hDRG from donors with (red) and without (grey) prior pain history.
(**R-T**) Summary graphs showing voltage sag (H), input-output curves (I), and rheobase (J).
(**R**) Voltage sag in response to hyperpolarizing current injections; p=0.0216 (not significant), Mann-Whitney test.
(**S**) Input-output curve showing number of spikes fired plotted against suprathreshold current injected. Mixed effects model analysis shows significant fixed effect of current injection (p=0.0021); fixed effects of pain history (p=0.2424) and the interaction of pain history x current injected (p=0.6400) were not significant.
(**T**) Rheobase; p=0.4334 (not significant), Mann-Whitney test.

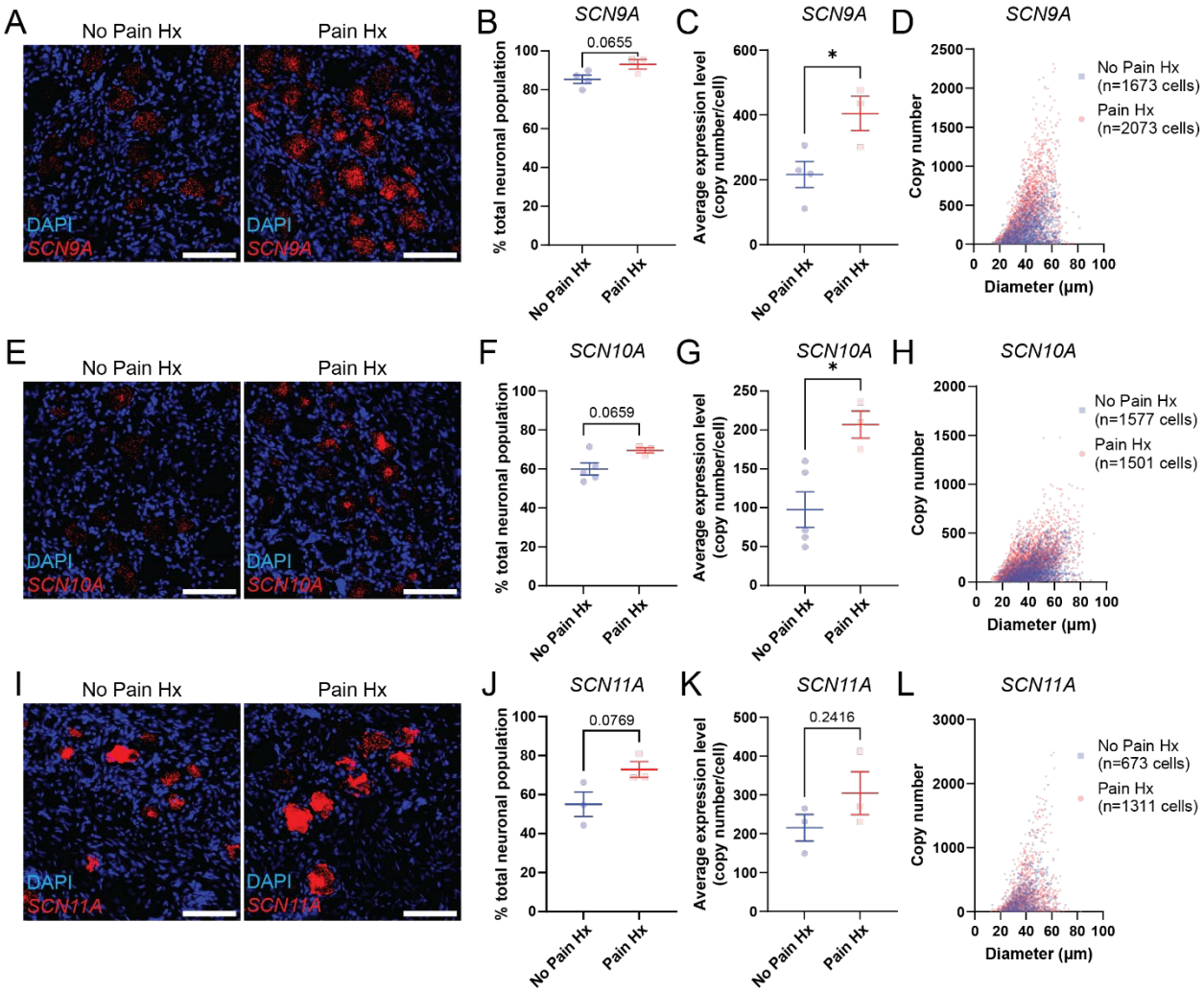

Fig. 6. Donors with pain history exhibit higher levels of *SCN9A* and *SCN10A* expression in hDRG compared to donors without pain history.

(**A**) Representative images of in situ hybridization for *SCN9A* (encoding Nav1.7, red) in hDRG sections from donors with (right) and without (left) significant history of pain. Scale bar = 100 µm.

(**B**) Summary graph of the proportion of *SCN9A*+ hDRG neurons between donors with and without prior pain history. P=0.0655, unpaired t-test. N=4 (No Pain Hx), 3 (Pain Hx).

(**C**) Summary graph of within-cell expression of *SCN9A* transcripts between donors with and without pain history. For each donor, the *SCN9A* copy numbers of all *SCN9A*-expressing neurons were averaged.

N=4 (No Pain Hx), 3 (Pain Hx); 331-946 *SCN9A*+ cells per donor. (*) p=0.0343, unpaired t-test.

(**D**) Scatter plot of *SCN9A* copy number vs. hDRG soma diameter for the two donor groups. N=1673(No Pain Hx), N=2073 (Pain Hx) neurons

(**E**) Representative images of in situ hybridization for *SCN10A* (Nav1.8, red), in hDRG sections from donors with (right) and without (left) significant history of pain. Scale bar = 100µm.

(**F**) Summary graph of the proportion of *SCN10A*+ hDRG neurons between donor groups. N=5 (No Pain Hx), 3 (Pain Hx); P=0.0659, unpaired t-test.

(**G**) Summary graph of within-cell expression of *SCN10A* between donor groups. N=5 (No Pain Hx), 3 (Pain Hx); 134-627 *SCN10A*+ cells per donor. (*) p=0.0161, unpaired t-test.

1272 (**H**) Scatter plot of *SCN10A* copy number vs. soma diameter for the two donor groups.
1273 N=1557(No Pain Hx), N=1501 (Pain Hx) neurons.
1274 (**I**) Representative images of in situ hybridization for *SCN11A* (Nav1.9, red), in hDRG sections
1275 from donors with (right) and without (left) significant history of pain. Scale bar = 100µm.
1276 (**J**) Summary graph of the proportion of *SCN11A*+ hDRG neurons between donor groups.
1277 P=0.0769, unpaired t-test. N=3 for both Pain Hx and No Pain Hx groups.
1278 (**K**) Summary graph of within-cell expression of *SCN11A* between donor groups (3 donors per
1279 group, 175-719 *SCN11A*+ cells per donor). P=0.2416, unpaired t-test. N=3 for both Pain Hx and
1280 No Pain Hx groups.
1281 (**L**) Scatter plot of *SCN11A* copy number vs. soma diameter for the two donor groups. N=673
1282 (No Pain Hx), 1311 (Pain Hx).
1283

List of Supplementary Materials

Supplementary Tables

Table S1. Detailed donor information (see separate Excel file)

Table S2. Comparison of Rheobase between hDRG neurons with different firing patterns

Table S3. DEG T-types (see separate Excel file)

Table S4. DEG E-types (see separate Excel file)

Table S5. Summary of donor demographic information, segmented by pain history

Table S6. Summary of electrophysiological features of E-type 1 between Pain Hx and No Pain Hx donors

Table S7. Summary of electrophysiological features of E-type 2 between Pain Hx and No Pain Hx donors

Table S8. Summary of electrophysiological features of E-type 3 between Pain Hx and No Pain Hx donors

Table S9. Statistics Table (see separate Excel file)

Supplementary Figures

Fig S1. Elbow plot showing the within-cluster sum of squares against different K values

Fig S2. E-type distribution across days in vitro

Fig S3. Additional membrane properties of hDRG E-types

Fig S4. Soma diameters across hDRG E-types

Fig S5. Quality control measures for hDRG Patch-seq data

Fig S6. Transcriptional clustering and T-type annotation of hDRG Patch-seq samples

Fig S7. E-type distributions are not affected by pain history

Fig S8. hDRG firing frequencies in E-type 1 separated by prior pain history

Supplementary Text: PRECISION Human Pain Network group members

Table S2. Comparison of Rheobase between hDRG neurons with different firing patterns

	High Rheobase	Single	Repetitive
N	30	97	101
Rheobase (Mean ± SEM)*	1707 ± 90.9 †,‡	942.2 ± 66.3 §	511.4 ± 45.4

*p<0.0001, Kruskall Wallis Test
† p<0.0001, Dunn's Multiple Comparison test, High Rheobase vs. repetitive
‡ p<0.0001, Dunn's Multiple Comparison test, High Rheobase vs. Single
§ p<0.0001, Dunn's Multiple Comparison test, Single vs. Repetitive

Table S5. Summary of hDRG donor characteristics, segmented by pain history

	No Pain Hx	Pain Hx
N	34	13
Race		
White	24	9
Black	9	3
Other/Unknown	1	1
Sex		
Male	20	8
Female	14	5
Cause of Death		
Anoxia	18	5
Stroke	11	5
Head Trauma	4	3
Other/Unknown	1	0
Age (years) †,(NS)	42.74±16.50	49.92±12.98
Body mass index †, (NS)	27.56±7.13	28.20±6.36

† Displayed in Mean ± SD
NS, Not significant; p>0.05, unpaired t-tests

Table S6. Summary of electrophysiological features of E-type 1 between Pain Hx and No Pain Hx donors

	No Pain Hx (n=26 cells)	Pain Hx (n=4 cells)	P-value
Resting membrane potential (mV)	-49.02 ± 1.59	-44.12 ± 5.52	0.46 †
Input resistance (MΩ)	89.11 ± 8.97	158.1 ± 65.87	0.33 †
Voltage sag ratio	0.24 ± 0.03	0.28 ± 0.12	0.69 ‡
Rheobase (pA)	1182.66 ± 94.98	1654.52 ± 176.74	0.0732 ‡
AP threshold (mV)	-6.46 ± 2.18	-10.95 ± 5.76	0.4597 ‡
AP Amplitude (mV)	27.78 ± 2.54	39.86 ± 4.24	0.0837 ‡
AP Peak (overshoot; mV)	21.32 ± 2.56	34.20 ± 11.03	0.10 ‡
Half-width (ms)	2.80 ± 0.29	2.73 ± 0.80	0.89 †
Rise time (ms)	1.08 ± 0.10	1.95 ± 0.96	0.51 †
Decay time (ms)	4.75 ± 0.49	3.16 ± 0.84	0.24 †

† Mann-Whitney test
‡ Unpaired t-test

Table S7. Summary of electrophysiological features of E-type 2 between Pain Hx and No Pain Hx donors

	No Pain Hx (n=43 cells)	Pain Hx (n=15 cells)	P-value
Resting membrane potential (mV)	-49.59 ± 2.09	-55.78 ± 3.42	0.14 ‡
Input resistance (MΩ)	157.12 ± 18.80	162.63 ± 23.52	0.54 †
Voltage sag ratio	0.30 ± 0.03	0.41 ± 0.03	**0.0046** †
Rheobase (pA)	323.05 ± 32.24	288.45 ± 46.55	0.87 †
AP threshold (mV)	-16.53 ± 1.25	-19.27 ± 1.77	0.25 ‡
AP Amplitude (mV)	65.73 ± 1.58	74.71 ± 1.89	**0.0022** †
AP Peak (overshoot; mV)	49.20 ± 1.16	55.44 ± 1.88	0.0078 ‡
Half-width (ms)	5.73 ± 0.40	4.59 ± 0.47	0.12 †
Rise time (ms)	0.84 ± 0.05	0.71 ± 0.04	0.16 †
Decay time (ms)	10.11 ± 0.65	8.84 ± 0.80	0.44 †

† Mann-Whitney test
‡ Unpaired t-test

Table S8. Summary of electrophysiological features of E-type32 between Pain Hx and No Pain Hx donors

	No Pain Hx (n=84 cells)	Pain Hx (n=19 cells)	P-value
Resting membrane potential (mV)	-54.73 ± 0.67	-52.44 ± 0.94	0.031 †
Input resistance (MΩ)	66.29 ± 6.47	50.83 ± 12.85	0.068 †
Voltage sag ratio	0.45 ± 0.17	0.53 ± 0.04	0.0216 †
Rheobase (pA)	1074.41 ± 76.77	1175.25 ± 144.95	0.43 †
AP threshold (mV)	-21.86 ± 1.92	-20.12 ± 1.92	0.78 †
AP Amplitude (mV)	71.90 ± 1.22	71.14 ± 2.41	0.79 ‡
AP Peak (overshoot; mV)	50.46 ± 1.08	51.02 ± 1.74	0.83 ‡
Half-width (ms)	2.31 ± 0.12	1.78 ± 0.19	0.0458 †
Rise time (ms)	0.73 ± 0.08	0.55 ± 0.05	0.074 †
Decay time (ms)	3.99 ± 0.21	2.96 ± 0.33	0.034 †

† Mann-Whitney test
‡ Unpaired t-test

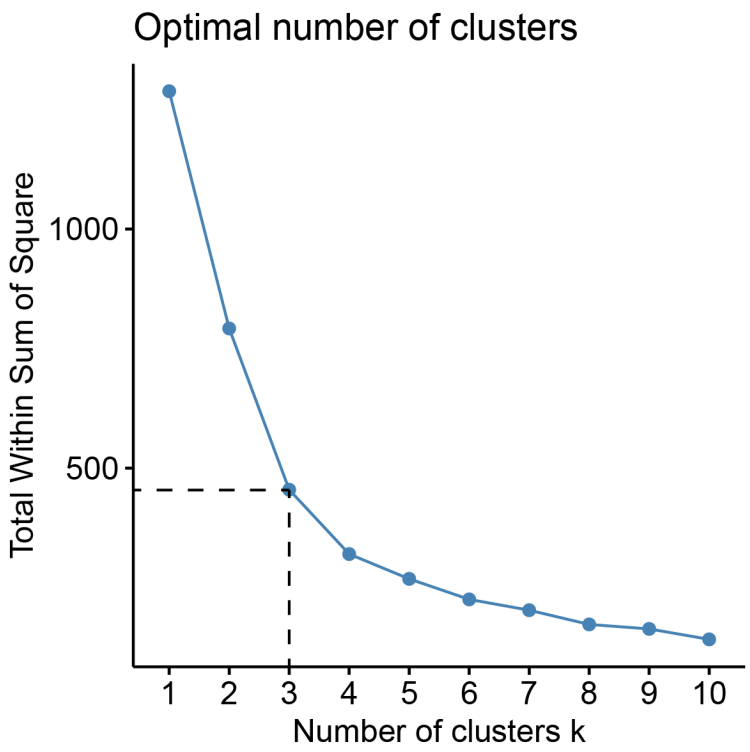

Fig S1. Elbow plot showing the within-cluster sum of squares against different K values.
We chose k=3 as the ideal cluster number for balancing model fit and complexity.

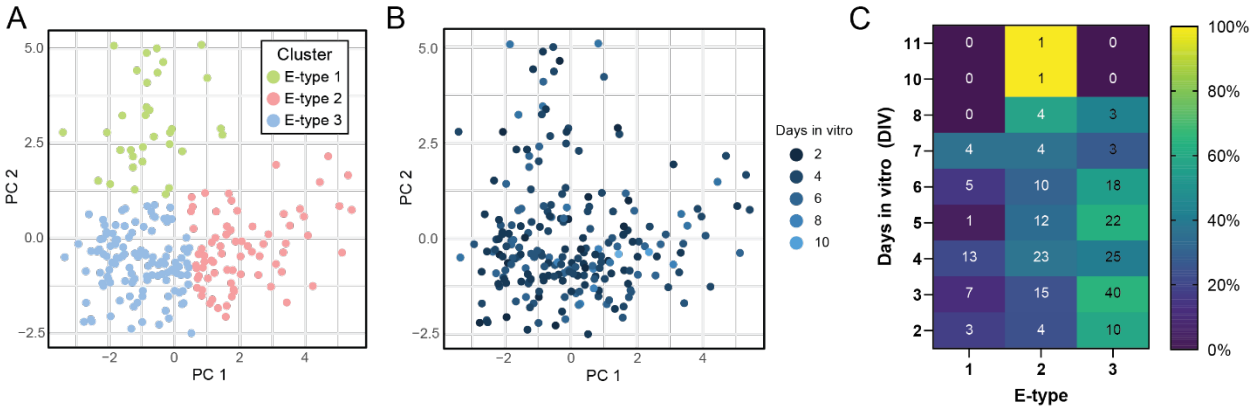

Fig S2. E-type distribution across days in vitro.

(**A**) Score plot of individual hDRG neurons clustered by their electrophysiological properties.

(**B**) Same plot in panel A, but each neuron is color-coded by the number of days in culture before recording.

(**C**) Heat map of E-type distributions across DIV. Number in each box shows number of cells corresponding to the E-type on the X-axis that were recorded at the DIV specified on the Y-axis. Each box is color-coded based on the relative proportion (%) of each E-type out of all the cells recorded on a particular DIV.

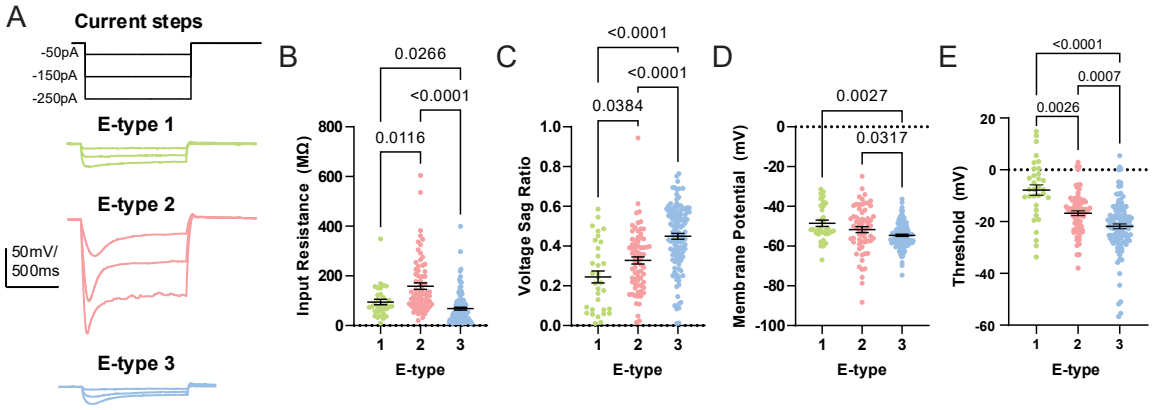

Fig S3. Additional membrane properties of hDRG E-types. (**A**) Example voltage traces of each hDRG E-type in response to 1 second hyperpolarizing current injection steps.
(**B-E**) Summary graphs of input resistance (**B**), voltage sag (**C**), resting membrane potential (**D**), and AP threshold (**E**) for each hDRG E-type. N=33 (E-type 1), 74 (E-type 2), and 121 neurons (E-type 3). Bonferroni correction for multiple comparisons were used to determine threshold for statistical significance (α=0.005) for group comparisons using Kruskall-Wallis or ANOVA tests. P-values for Dunn's post-hoc test (Kruskall-Wallis) or Tukey's post-hoc test (ANOVA) are shown in plot.
(**B**) Input resistance, p<0.0001 (significant), Kruskall-Wallis test.
(**C**) Voltage sag ratio, , p<0.0001 (significant), one-way ANOVA.
(**D**) Resting membrane potential, p<0.0001 (significant), Kruskall-Wallis test.
(**E**) AP threshold, p<0.0001 (significant), Kruskall-Wallis test.

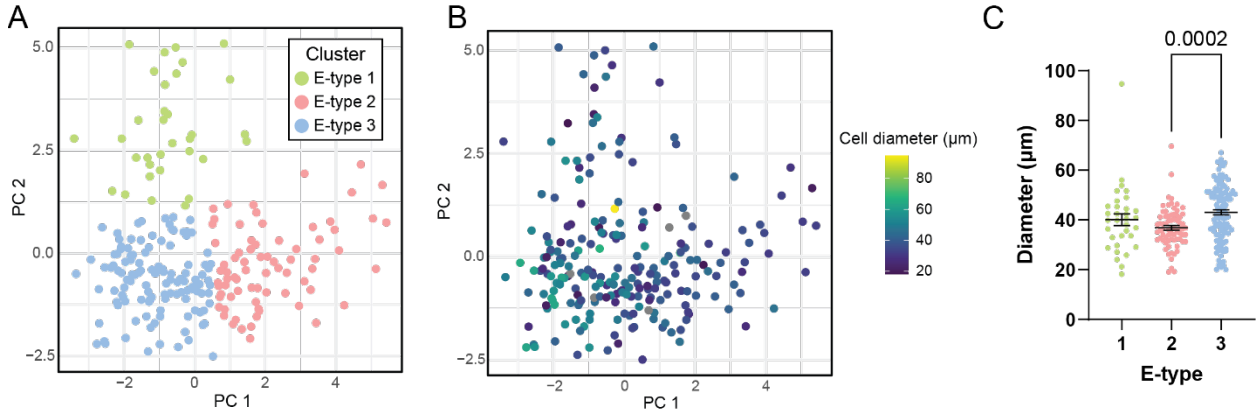

Fig S4. Soma diameters across hDRG E-types.

(**A**) Score plot of individual hDRG neurons clustered by their electrophysiological properties.

(**B**) Same PCA plot in (**A**) color-coded by a heat map of soma diameters in microns.

(**C**) Summary graph of soma diameter for each hDRG E-type. P=0.0003, Kruskall-Wallis test. N=33 (E-type 1), 74 (E-type 2), and 119 neurons (E-type 3). Post-hoc comparisons: p=0.0002, E-type 2 vs. E-type 3; p=0.6449, E-type 1 vs. E-type 2; p=0.2671, E-type 1 vs. E-type 3; Dunn's post-hoc test.

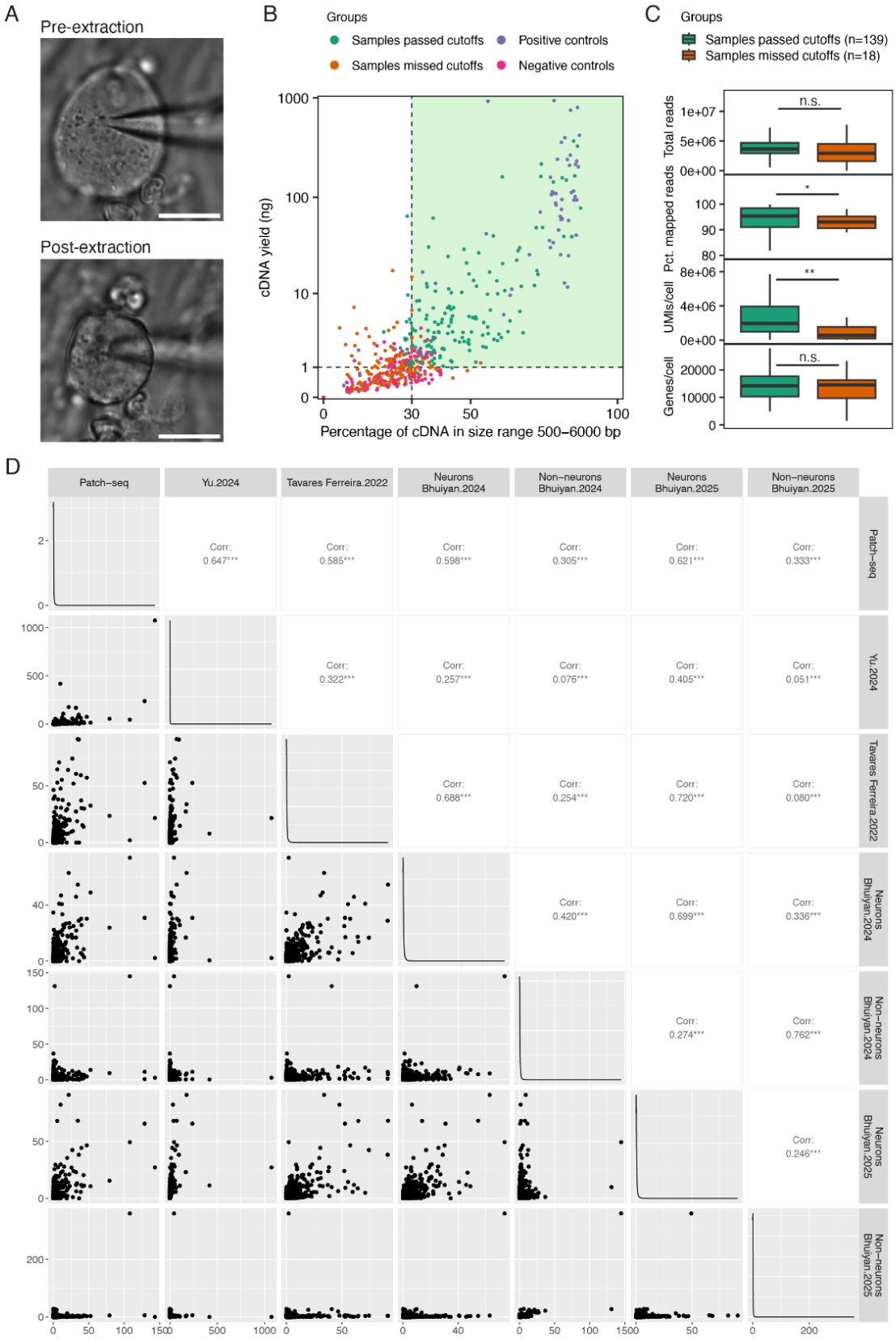
A
Pre-extraction
Post-extraction
B
Groups
Samples passed cutoffs
Samples missed cutoffs
Positive controls
Negative controls
cDNA yield (ng)
Percentage of cDNA in size range 500–6000 bp
C
Groups
Samples passed cutoffs (n=139)
Samples missed cutoffs (n=18)
Total reads
Pct. mapped reads
UMIs/cell
Genes/cell
n.s.
*
**
n.s.
D
Patch–seq
Yu.2024
Tavares Ferreira.2022
Neurons Bhuiyan.2024
Non–neurons Bhuiyan.2024
Neurons Bhuiyan.2025
Non–neurons Bhuiyan.2025
Corr: 0.647***
Corr: 0.585***
Corr: 0.598***
Corr: 0.305***
Corr: 0.621***
Corr: 0.333***
Corr: 0.322***
Corr: 0.257***
Corr: 0.076***
Corr: 0.405***
Corr: 0.051***
Corr: 0.688***
Corr: 0.254***
Corr: 0.720***
Corr: 0.080***
Corr: 0.420***
Corr: 0.699***
Corr: 0.336***
Corr: 0.274***
Corr: 0.762***
Corr: 0.246***

Fig. S5. Quality control measures for hDRG Patch-seq data.

(**A**) Example images of cytosolic content extraction from a recorded neuron. Shrinkage of the soma size can be confirmed visually during the extraction process. Scale bar = 30 μm.

(**B**) QC metrics of the cDNA library prepared from Patch-seq samples. Samples with cDNA yield > 1 ng, at least 30% of cDNA within the size range 500-6000 bp, and both cDNA yield and cDNA percent in range are at least 25% higher than associated negative controls are considered as high quality and proceed to library preparation and sequencing. Positive controls are prepared from 50 ng of total mouse brain RNA. Negative controls are prepared from either internal solution or nuclease-free water.

(**C**) Sequencing metrics of the Patch-seq samples that passed the cDNA QC (n = 139) compared to the ones that failed QC (n = 19). N.s., Not significant. Total reads: p=0.1011, two-way student T-test. Percent of mapped reads: p=0.0320, two-way student T-test. UMIs: p=0.0064, two-way student T-test. Number of genes: p=0.5522, two-way student T-test.

(**D**) Pairwise correlation of hDRG Patch-seq data and published human DRG cell atlas. Bottom left panels show the normalized counts (log2CPM) of individual genes in two datasets, each averaged across all cells/nuclei in the indicated cell population from the dataset. Top right panels show the Pearson's correlation coefficient based on the average expression of genes between dataset pairs.

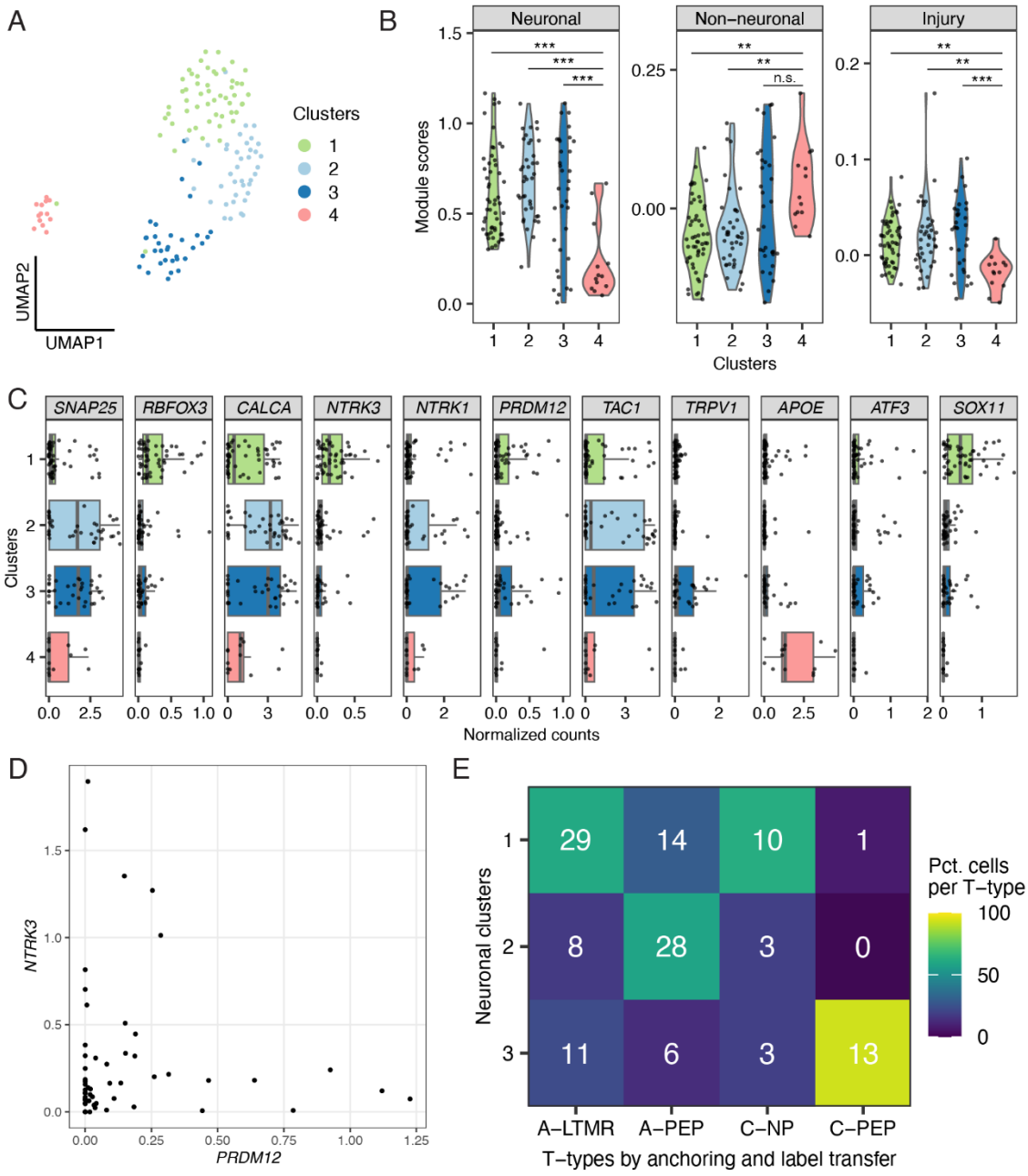

Fig S6. Transcriptional clustering and T-type annotation of hDRG Patch-seq samples. (**A**) UMAP of 139 Patch-seq samples, colored by transcriptional clusters. Cluster 1 (n = 54), cluster 2 (n = 39), cluster 3 (n = 33), cluster 4 (n = 13).
(**B**) Violin plots showing the module scores in samples from different transcriptional clusters. Module scores were generated by aggregating the expression levels of top 200 marker genes identified from publicly available datasets (see Methods). One-way ANOVA tests, p = 3.5e-06 (***) for neuronal module score, p = 0.000491 (***) for non-neuronal module score, and p = 0.000872 (***) for injury module score.

(**C**) Normalized counts (log_2CPM) of select hDRG cell class marker genes in each transcriptional cluster. Scatter plot indicats the expression in individual samples and the boxes indicate quartiles and whiskers are 1.5-times the interquartile range (Q1-Q3). The median is a grey line inside each box.
(**D**) Scatter plot showing the normalized counts (log_2CPM) of A-LTMR transcription factor *NTRK3* and C-fiber transcription factor *PRDM12* in individual Patch-seq samples from cluster 1.
(**E**) Heatmap showing the percent (as the color gradient) and cell counts (as numbers on the heatmap) of Patch-eq samples in each transcriptional neuronal cluster (clusters 1-3) that are assigned to T-types identified by anchoring to hDRG single-soma RNA-seq data.

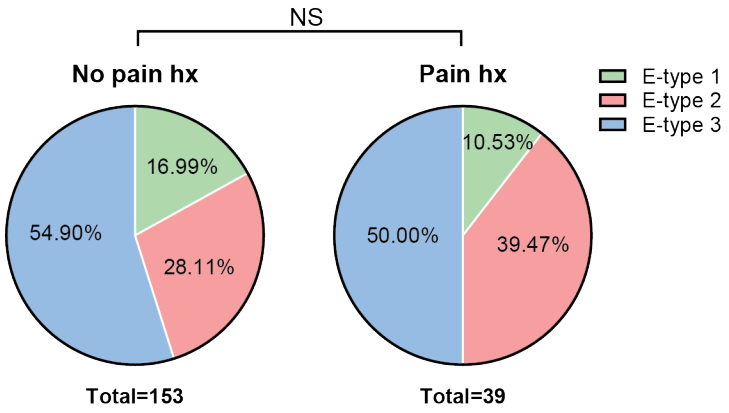

Fig S7. E-type distributions are not affected by pain history. Pie charts of the relative proportion of each hDRG E-type in donors with (Pain hx, right) and without (No pain hx, left) prior pain history. NS, not significant. Chi-square test, p=0.4540. N=153 neurons (No Pain Hx) and 39 neurons (Pain Hx).

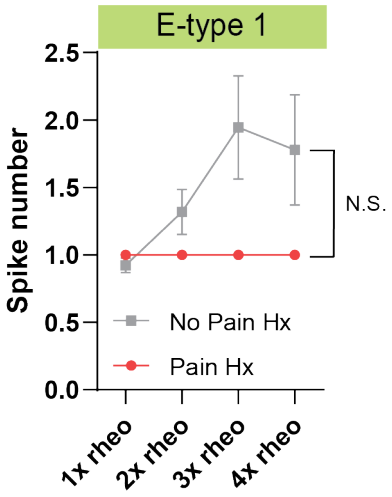

Fig S8. hDRG firing frequencies in E-type 1 separated by prior pain history. Input-output curves of AP frequency vs depolarizing current injections (1-4x rheobase) in hDRG with E-type 1 obtained from donors with (red; n=4 neurons) or without (grey; n=26 neurons) prior pain history. N.S., not significant. Mixed effects model analysis shows no significant fixed effect of current step (p=0.5921), pain history (p=0.2970), or interaction of current step x pain history (p=0.5921).

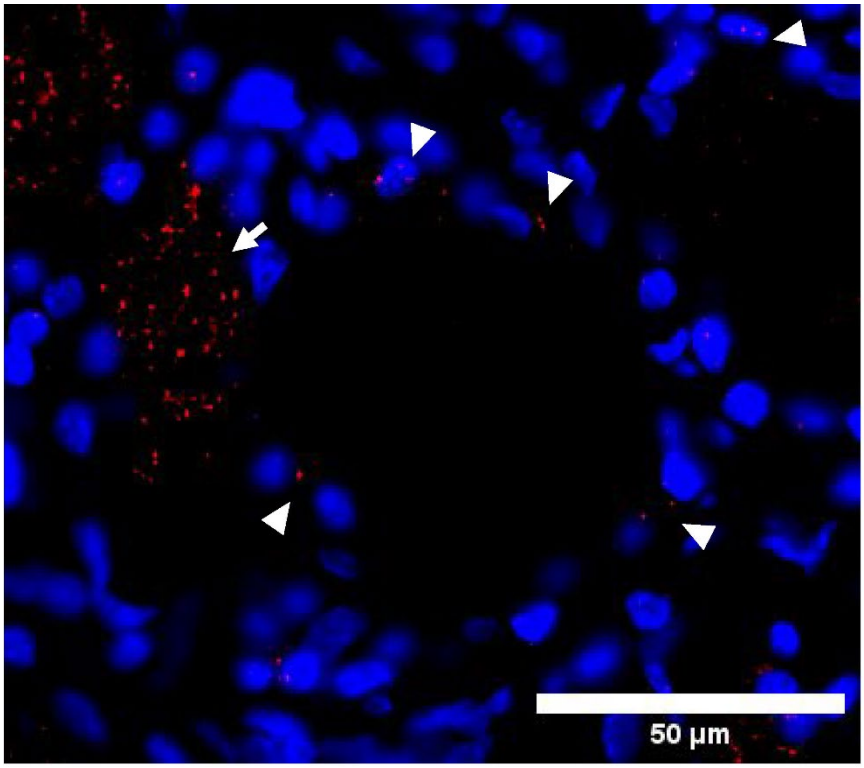

Fig S9. *SCN9A* expression in satellite glial cells. Arrowheads point to mRNA probes detected in satellite glial cells that surround the hDRG neuronal cell bodies. Arrow point to an adjacent neuron that expresses *SCN9A*. Blue=DAPI, red=*SCN9A* transcripts.

Supplementary Text: PRECISION Human Pain Network group members

The members of the NIH PRECISION Human Pain Network are: Abby Pei-ting Chiu, Allison M Barry, Amy Anderson, Asta Arendt-Tranholm, Andi Wangzhou, Ayesha Ahmad, Cathryn Payne, Christoph Paul Hofstetter, Claudio Tatsui, Diana Tavares Ferreira, Felipe Espinosa, Gregory O Dussor, Ishwarya Sankaranarayanan, Jeffrey Jarvik, Joseph B Lesnak, Juan Pablo Cata, Judith A Turner, Karen Segar, Katelyn Sadler, Katherin Althea Gabriel, Khadijah Mazhar, Marisol Mancilla-Moreno, Megan L Uhelski, Michael D Burton, Michele Curatolo, Muhammad Saad Yousuf, Nguyen Tran, Olivia Catherine Davis, Patrick M Dougherty, Robert Yates North, Stephanie Shiers, Theodore J Price, Úrzula Franco-Enzástiga, William Renthal, Evangelia Semizoglou, Shamsuddin A. Bhuiyan, Parth Bhatia, Dustin Griesemer, Erika K. Williams, Jiaxiang Wang, Lily S He, Hannah MacMillan, Clifford Woolf, Barbara Gomez, Aakansksha Jain, Selwyn Jayaker, Brian Wainger, Sanghun Lee, Xianjun Dong, Weiqiang Liu, Himanshu Chintalapudi, Anthony Cicalo, Jeffrey Moffitt, Hao Zhang, James R. Stone, Iris A Lopez, Kyle Eberlin, Floris V. Raasveld, Kevin Spiegler, Wenqin Luo, Huasheng Yu, Eric A. Kaiser, Caitlin E. Cronin, Ebenezer Simpson, Hao Wu, Julie Leu, Dongming Liang, Ying Li, Mingyao Li, Hanying Yan, Patrik Ernfors, Dmitry Usoskin, Hakan Olausson, Saad Nagi, Katarina Laurell, Maria Bograkou, Otmane Bouchatta, Ewa Jarocka, Johan Nikesjo, Robert W. Gereau IV, Bryan A. Copits, Rakesh Kumar, Grace E. Moore, Deblina Nandi, Kesav Kothapalli, David M Brogan, Christopher J Dy, Lite Yang, Juliet Mwirigi, John S Del Rosario, Jun-Nan Li, Prashant Gupta, Adam Dourson, Maria Payne, Alexander Chamessian, Gary F. Marklin, John A Lemen, Elvisa Mehinovic, Zitian Tang, Jenna Ulibarri, Emma Casey, Zefan Li, Brian Yu, Sheng Chih Jin, Kevin Boyer, Ibrahim Olabayode Saliu, Bijesh George, George Murray, Huma Naz, Guoyan Zhao, Valeria Cavalli, Pauline Meriau, Sarah F. Rosen, Isabelle Gordon, Jeffrey Milbrandt, Aaron DiAntonio, Aldrin KY Yim, Amy Strickland, Liya Yuan, Joseph A Bloom, Richard Slivicki, Jyl Boline, Sam Kessler, Joost Wagenaar, Maryann Martone, Sue Tappan